An Experimental and Numerical Investigation of Performance of Nanofluids

A Dissertation Submitted
in partial fulfillment of the requirements
for the degree of

Master of Engineering
in
Thermal Engineering

by

Richa Gupta

Registration No.: 801583020

Under the supervision of

Dr. Anu Mittal
Assistant Professor

Mr. Kundan Lal
Assistant Professor

MECHANICAL ENGINEERING DEPARTMENT
THAPAR UNIVERSITY, PATIALA

July, 2017

Certificate

I hereby declare that the thesis entitled "**An Experimental and Numerical Investigation of Performance of Nanofluids**" is an authentic record of my own work carried out as per the requirements for the award of the degree in **Master of Engineering** in **Thermal Engineering** at **Thapar University, Patiala** under the supervision of **Dr. Anu Mittal (Assistant Professor)** and **Mr. Kundan Lal (Assistant Professor)**, Mechanical Engineering Department Thapar University, Patiala during July, 2015 to July, 2017. No part of the matter embodied in this thesis report has been submitted to any other university or institute for the award of any degree.

Date: 14/07/2017

Richa

Richa Gupta

It is certified that the above statement made by the student is correct to the best of my /our knowledge and belief.

Anu Mittal

Dr. Anu Mittal
(Assistant Professor)
Mechanical Engineering Department
Thapar University, Patiala-147004

Mr. Kundan Lal
(Assistant Professor)
Mechanical Engineering Department
Thapar University, Patiala-147004

i

Dedicated to

My Parents

Acknowledgement

Writing this thesis has been fascinating and extremely rewarding. I would like to thank a number of people who have contributed to the final result in different ways.

To commence with, I pay my obeisance to my dear ones and my family who bestowed upon me good health, courage, inspiration and zeal. After that I express my sincere and deepest gratitude to my supervisors, Mr. Kundan Lal & Dr. Anu Mittal, Assistant Professor Department of Mechanical Engineering, Thapar University. Their expertise, invaluable guidance, constant encouragement, affectionate attitude, understanding, patience and healthy criticism added considerably to my experience. Without his continual inspiration, it would have not been possible to complete this study.

I take this opportunity to express my deep sense of gratitude and respectful regards to Dr. J.S. Saini, Assistant Professor Department of Mechanical Engineering, Thapar University whose immense support and guidance made this possible.

I sincerely admire the contribution and thanks to my friends Vikas, Nishant Kumar, Manu Dev and Bhoopendra Pandey for their valuable support and also thanks to all of them who helped me directly or indirectly during this this study.

Richa Gupta

Abstract

Literature report shows that nanofluids have potential to perform as effective coolants as compared to the conventional coolants. This unique feature of nanofluids is due to their improved thermo physical properties. The thermal conductivity is one of them which has comparatively more significance. A significant amount of work has been also reported by various researchers on the thermal conductivity enhancement of nanofluids. There are many static as well as dynamic models which have been suggested to measure the thermal conductivity of variety of nanofluids. In addition to the fundamental studies about such variety of models, a very limited work has been reported about the numerical investigation of performance of such nanofluids.

In the present work, an attempt has been made to investigate into the behavior of a particular type of flow of nanofluid on a vertical flat plate. The problem has been well formulated by imposing the suitable boundary conditions. Subsequently to this, fundamental governing equation have been written using the properties of nanofluid for the flow of nanofluid along the vertical plate. In this arrangement, the general governing equations for the flow over a flat plate and thermo physical property equations about the performance of nanofluids have been coupled together. All the equations are solved together to obtain the final partial differential equations. These equations are expressed in term of transformed coordinates. The resulting non-linear partial differential equations were solved using finite element method with the help of MATLAB. The temperature distribution across the vertical plate has been investigated and plotted. The results seem to follow the expected variations.

In second part of the work, the thermal conductivity of Al_2O_3-H_2O nanofluid has been investigated against volume fraction of nanoparticles into base fluid and temperature rise. A thermal property analyzer (KD2 Pro) has been used to measure the thermal conductivity of different samples nanofluid. The experimentation has been conducted only up to 60°C. The results obtained have been compared with some of the fundamental models. From the experimental results, it was observed that the thermal conductivity ratio, K_{nf}/K_f increases with increase in temperature as well as with volume fraction (0.01 to 0.08).

Keywords: Thermal conductivity, nanofluid, numerical study, experimental study, KD2 pro

Contents

Certificate ..... Error! Bookmark not defined.

Abstract ..... **iv**

List of Figures ..... **vii**

List of Tables ..... **viii**

Nomenclature ..... **ix**

Chapter 1 Introduction **1**

1.1 Introduction 1

1.2 Objectives: 6

Chapter 2 Literature Review **8**

Chapter 3 Numerical Investigation into Performance Of Nanofluid. **16**

3.1 Mathematical analysis of heat transfer enhancement along a vertical plate using nanofluid 16

3.2 Non-dimensionlisation of the equation- 17

3.3 Transformation of the boundary conditions 20

3.4 Method of solution 20

3.4.1 Finite element method 20

3.4.2 Generation of the element equation 21

3.4.3 Grouping of Element Equations 21

3.4.4 Imposition of boundary conditions 21

3.4.5 Solution of assembled equation 21

3.4.6 The corresponding boundary conditions becomes: 21

3.4.7 Variational formulation 22

Chapter 4 Experiment, Material & Method **34**

4.1 Test Facility at Thapar University and Experimental procedure 34

4.2 Nanomaterial 34

4.3 Preparation of nanofluid: Sonicater 34

4.4 Thermal Property analyzer 35

Chapter 5 Results and Discussions 40

5.1 Experimental Results 40

Chapter 6 Conclusion & Future Scope 48

6.1 Conclusion 48

6.2 Future Scope 48

References 50

Appendix **54**

List of Figures

Figure No.	Title of the Figure	Page No.
Figure 3.1	Geometry and co-ordinate system	17
Figure 3.2	Rectangular finite element	24
Figure 3.3	Nodal presentation of the problem	26
Figure 3.4	3-D graph between theta and eta	32
Figure 3.5	Two-dimensional graph between theta and eta	33
Figure 3.6	Comparison between models of thermal conductivity	33
Figure 4.1	Oscar ultrasonicator	35
Figure 4.2	KD2 Pro	36
Figure 4.3	KS-1 sensor needle	37
Figure 4.4	TR-1 sensor needle	38
Figure 4.5	SH-1 sensor needle	39
Figure 5.1	Variation of Thermal Conductivity of water with temperature	41
Figure 5.2	Variation of Mean Thermal Conductivity of water with temperature	42
Figure 5.3	Thermal Conductivity of Al_2O_3-H_2O at 1% & 2%volumetric concentration	43
Figure 5.4	Comparison of Experimental data at (0.01) vol.concentration with empirical Models	44
Figure 5.5	Comparison of Experimental data at(0.02) vol. concentration with empirical Models	45
Figure 5.6	Thermal Conductivity of Al_2O_3-H_2O at different volumetric concentration	46
Figure 5.7	Comparison of Experimental data at (30°C) with empirical models for different vol. concentration	47
Figure 5.8	Comparison of Experimental data at (40°C) with empirical models for different vol. concentration	48

List of Tables

Table No.	Name of the table	Page No.
Table 1.1	Comparison of microparticles and nanoparticles	2
Table 1.2	Thermal Conductivity of various materials at 300K	3
Table 3.1	Thermo physical properties of water and nanoparticle	26

Nomenclature

Roman

K_{nf}	Thermal Conductivity of nanofluid
K_f	Thermal Conductivity of base fluid
Pr	Prandtl Number
Ri	Dimensionless buoyancy parameter
Gr	Grashoff Number
(x,y)	Cartesian coordinates
Tw	Temperature on the plate
T_∞	Ambient temperature attained
G	Gravitational acceleration
φ	Volume fraction of nanoparticle
u , v	Velocity component in the x , y direction
u_∞	Free stream velocity
Q	Dimensionless heat source/sink parameter
Q_0	Volumetric rate of heat generation
F	Dimensionless stream function
H	Dimensionless velocity function
$J_{p,\,T}$	Nanoparticle mass flux due to thermophoresis
$J_{p,B}$	Nanoparticle mass flux due to to Brownian diffusion
M	Viscosity

Greek symbols

ρ_f	Fluid density
ρ_{nf}	Nanofluid density
Ψ	Stream Function
Y	Kinematic viscosity of the fluid
B	Volumetric expansion coefficient of the fluid
$\theta(\xi,\eta)$	Dimensionless temperature
$\boldsymbol{\xi}$,$\boldsymbol{\eta}$	Transformed variables

Subscript

Symbol	Notation
w , ∞	Condition at the wall and infinity, respectively
Nf	Nanofluid
F	Base fluid

Chapter 1

Introduction

1.1 Introduction

Nanofluid is a fluid that contains nano-particles and base fluid. Solid particles have higher thermal conductivity in comparison to that of liquid. Present day nanotechnology can create metallic or nonmetallic nanoparticles which have extraordinary mechanical and thermal properties. The normally used nanoparticle materials and base liquids are as follows (Das et al., 2007)

Nanoparticles utilized as a part of nanofluids are made of different materials, for example, metal oxide ceramic (Al_2O_3, CuO, TiO_2), Metals (Cu, Ag, Au), nitride ceramics (SiN), Carbide ceramics (SiC, TiC), semiconductors (TiO_2, SiC), carbon nanotubes, filaments and composite materials, for example, alloyed nanoparticles $Al_{70}Cu_{30}$. Notwithstanding metallic, nonmetallic and different materials for nanoparticles, totally new structures, for example, materials doped with molecules in their solid- fluid interface structure (Cerium Oxide, Calcium doped Nano powder, CeO_2/Ca) may likewise have desirable features. Many sorts of fluids, for example, water; ethylene glycol and oil have been utilized as host fluids in nanofluids. Likewise of conventional fluids, the nanoparticles may likewise be scattered in bio-liquids and polymer solution (other mechanical application to have reasonable properties). Nanofluids usually have nanoparticles with its sizes ranging up to 100 nm. This is stated, in light of the fact that in the nano scale range, essential properties of nanofluids depend firmly on molecular size, shape and its surface interface area (Masuda et al., 1993). Nanofluids are being utilized to accomplish high performance cooling in different enterprises.

The conventional approach to improve heat transfer in different thermal system is to expand the heat transfer surface area of cooling gadgets which can easily be clarified by the accompanying expression (Saidur et al., 2011)

$$\breve{Q} = \dot{h}\,\dot{A}\,\Delta T \tag{1.1}$$

Where $\breve{Q}$ is the heat flow, $\dot{h}$ is the heat transfer coefficient, $\dot{A}$ is the heat transfer area Furthermore, ΔT is the temperature difference that results in the heat flow. So as to build the heat flow, greater temperature distinction must be kept up by diminishing the temperature of coolant which may bring about the lessening of efficiency. Therefore, expanding the heat

exchange territory is a common methodology to enhance the heat exchange area which may prompts undesirable increment of weight of the system. Notwithstanding, this procedure can't be utilized in microchips and micro electro mechanical systems (MEMS) in light of their smaller than normal size. Conventional method also has some limitations. The thermal conductivity of the nanofluids is more than that of the regular heat transfer fluids. The main properties of nanofluids which make them significant as the next generation flow and heat transfer fluids are as follows (Das et al., 2007; Pfautsch et al., 2008)

- Due to small size blockage of `channel and erosion in channel walls are no longer issue. Nanoparticles stay suspended much longer than mm –or –μm-sized particles.
- The surface area per unit volume (SSA) of nanoparticles is more than that of micro-practicles. This can be easily explained by the following expression:

$$\text{SSA} = \frac{\text{particle surface area}}{\text{particle volume}} = \frac{\pi d_p^2}{\left(\frac{\pi}{6}\right) d_p^3} = \frac{6}{d_p} \tag{1.2}$$

- These properties can be utilized to form stable suspensions with enhanced flow and heat transfer.
- Less pumping power is required because of small nano size as compared to micro size.

Table 1.1 Comparison of microparticles and nanoparticles (Das et al., 2007)

	Microparticles	**Nanoparticles**
Stability	Settle	Stable(remain in suspension almost indefinitely)
Surface/volume ratio	1	1000 times larger than that of microparticles
Conductivity	Low	High
Clog to micro channel	Yes	No
Erosion	Yes	No
Pumping Power	Large	Small
Nanoscale Phenomena	No	Yes

Nanofluids provides a great deal of interest with their high potential to provide good performance properties, particularly in terms of heat transfer enhancement. It is well known that at room temperature, metals in solid form have higher thermal conductivities than those in liquid state as shown in Table 1.1. The thermal conductivity of metallic fluids is substantially more prominent than that of nonmetallic fluids. Therefore, the thermal conductivity of liquids that contain suspended strong metallic particles could be expected to be significantly higher than those of regular heat transfer liquids.

Table 1.2: Thermal conductivity of various materials at 300 K

Classification	Material	Thermal-Conductivity (W/mk)
Metallic solids	Silver Copper Aluminum	429 401 237
Nonmetallic solids	Diamond Carbon nanotubes	3300 3000
	Silicon Alumina	148 40
Metallic liquids	Sodium at 644k	72.3
Nonmetallic liquids	Water Ethylene glycol Engine oil	0.613 0.253 0.145

In the course of the most recent seven years, various trial and a couple of hypothetical papers have been showed up offering nanofluid property estimations and models portraying the key material science of improved thermal conductivities for various nanoparticle-and-fluid blending. Despite the fact that the trial comes about have shown a noteworthy potential for thermal conductivity upgrade, the assurance of the fundamental material science is still in an essential stage, muddled by the way that the accessible exploratory information from various research bunches does not coordinate altogether. Specialists have explored the thermal characteristics containing different nanoparticles, for example, copper oxide, aluminum oxide, titanium oxide, copper and carbon nanotubes. Scattering of a very small amount of nanotubes produces a noteworthy change in the effective thermal conductivity of host fluid. The base liquids are ordinarily water, mixture of water with ethylene glycol and engine oil, however it relies on the type of application it is used for. Nanofluids generally contains 5% volume fraction of nanoparticles to seek powerful properties over the base fluid. These trademark features of nanofluids make them proper for the up and coming era of flow and heat-transfer liquids. Also, nanofluids possess some new characteristics compared to fluids which are as follows:

- Enhancement in thermal conductivity of nanofluids at low nanoparticle concentration.
- Enhancement in thermal conductivity of nanofluids with decrease in the size of nanoparticle.
- Enhancement in thermal conductivity of nanofluids with temperature.
- Non-linear increase in thermal conductivity of nanofluids with nanoparticle concentration.

Nanofluids are generally prepared by the two fundamental methods (Das et al., 2007; Pfautsch et al., 2008; Yu et al., 2012). They are two –step method and one-step method.

Two-step method is the widely used method for preparing nanofluids. In this method, first the nanoparticle, nanotubes are obtained as dry powers by either physical or chemical methods and then the nano sized powder are diffused into the base liquid with the help of homogenizing, high-shear mixing and ultrasonic agitation. It is one of the most economical methods to produce nanofluids on a large scale. The real drawback of the two stage process is that the nanoparticles tend to agglomerate because of high surface area and surface movement. Also, due to trouble in getting stable nanofluids by two-step method, some procedures are provided which incorporates one-step method.

In one-step method, direct evaporation and condensation of the nanoparticle materials in the base liquid are required to deliver stable nanofluids. The vacuum–SANSS (submerged arc nanoparticle blend framework) is one of the effective physical technique for recent interest. One-step physical strategy can't blend nanofluids at large scale and also the cost of planning is additionally high. The one-step process is positive since it forestalls oxidation of the nanoparticles. The disadvantage of one-step method is the residual reactants that remain within the nanofluids because of their incomplete reaction. For the computational and mathematical models detailed in this area incorporate two principles –approaches as: Nanofluids are single phase fluids in which, the solid particles behave as fluids. Classical theory of single phase fluids can be applied on nanofluids, in which their physical properties are taken as the functional properties of both, constituents and their concentrations. Now a days, viscosity and thermal conductivity of nanofluids can be calculated by experimental correlations. An optional approach recreates nanofluids utilizing a general two-component non-homogeneous balance model for transport phenomena. It is critical to comprehend the system by which the nanoparticles can build up a slip velocity concerning the base liquid. The seven important mechanisms responsible for this slip velocity have been mentioned by (Bungiorno et al., 2006), to derive the conservation equations for nanofluids.

These are given as follows:

The irregular movement of nano molecule inside the base liquids is called Brownian motion which results from continuous impact between the nanoparticles and the particles of the base liquid. Brownian motion is determined by the Brownian diffusion coefficient, which is given by the Einstein-Stokes equation (Buogiorno et al., 2006)

$$D_B = \frac{k_B T}{3\pi\mu_{nf} d_p} \tag{1.3}$$

In the case of water based nanofluids with nanoparticles diameter 1-100nm, the Brownian diffusion coefficient ranges from 4×10^{-10} m^2/ s to 4×10^{-12} m^2/s at room temperature [Buogiorno et al., 2006]. By knowing the value of diameter of nanoparticle and viscosity of nanofluids, the diffusion coefficient can be determined. The nanoparticle mass flux ($J_{P,B}$) due to Brownian motion can be calculated as (Buogiorno et al., 2006)

$$J_{P,B} = -\rho_P D_B \nabla\varphi \tag{1.4}$$

Small size particles suspended in the fluid can disperse under the effect of temperature gradient. This phenomenon is called thermophoresis or soret effect. The thermophoretic velocity can be found (Buogiorno et al., 2006) as

$$V_T = -\hat{\beta}\,\frac{\mu_{nf}}{\rho_{nf}}.\frac{\nabla T}{T} \tag{1.5}$$

Where the proportionality factor, is given by (Buongiorno et al., 2006; McNab et al., 1973)

$$\hat{\beta} = 0.26\frac{k_{nf}}{2k_{nf}+k_p} \tag{1.6}$$

The nanoparticle mass flux ($J_{P,T}$) due to thermophoretic effect can be calculated as (Buogiorno et al., 2006)

$$J_{P,T} = \rho_P \varphi V_T = -\rho_P D_T \frac{\nabla T}{T} \;\; with\; D_T = \beta\frac{\mu}{\rho}\varphi \tag{1.7}$$

The coefficient DT_{is} referred as the thermal diffusion coefficient.

If there should be an occurrence of turbulent flow, a molecule dispersed in a liquid could build up a slip velocity because of its inertia. The slip velocity because of turbulent eddies, V_e, can be gotten from the condition of movement (Buogiorno et al., 2006)

$$\frac{\pi}{6}d_p^3\rho_p\frac{dV_e}{dt} = -3\pi d_p\mu_{nf}V_e \;\; with \;\; V_e = V_{eoe^{-t/\tau_p}} \; with\; \tau_p = \frac{\rho_p d_p^2}{18\mu_{nf}} \tag{1.8}$$

This effect can be neglected in the case of laminar flow.

A nanoparticle diffused in a liquid in which a concentration gradient exists, is exposed to a net force acting toward the path opposite to that gradient. This phenomenon is known as

diffusiophoresis. It is brought about by the effect of the molecule with the diffusing species. Notwithstanding, the base liquid of nanofluids is typically a one-segment substance with no concentration gradients. In this way, nanoparticle diffusiophoresis does not occur. But in case of Nanofluid containing with solute particle (salt water as base fluid), diffusion of salt particle causes nanoparticle to move in the fluid. Then, this slip mechanism cannot be neglected.

Under the influence of the shear stress, a molecule pivots around an axis perpendicular to the main flow direction. In the event that a relative axial velocity exists between the molecule and the liquid, a force opposite to the fundamental flow heading will emerge. This is known as the Magnus effect (Buongiorno et al., 2006; Sacithiri et al., 2011). In laminar stream, the relative axial velocity of nanoparticles is relied upon to be low. Subsequently, for nanoparticles the Magnus impact ought to be insignificant. As a molecule methodologies the wall, There is a resistance created by the weight in depleting liquid film between the nanoparticle and wall. This impact ends up plainly critical when the separation between the molecule and the wall is of the request of the molecule measurement. As a result of low nanoparticle volume division, it has no noteworthy impact. The nanoparticle settling speed because of gravity can be computed from an adjust of the buoyancy and viscous forces (Buongiorno et al., 2006)

$$\frac{\pi}{6} d_p^3 \left(\rho_p - \rho_{nf}\right) g_e = 3\pi d_p \mu_{nf} V_g \quad with \ V_g = \frac{(\rho_p - \rho_{nf}) d_p^2}{18\mu_{nf}} \tag{1.9}$$

In case of nanoparticle size (<100nm), the value of $V_g < 1.6\times10^{-8}$ m/s.

There are so many empirical models. They are particle and fluid specific. A very limited work has carried out to fundamental understand the behavior of nanofluid. In view of this an attempt has been made to solve the governing equation (partial, non-linear equation) using property of nanofluid.

1.2 Objectives:

- To formulate the governing equations for flow of heat transfer between vertical flat plate and nanofluid flowing over it.

- To solve the governing equations for the temperature distribution using FEM and MATLAB.
- Experimentally investigate the thermal conductivity of nanofluid.

Chapter 2

Literature Review

This chapter presents researchers work performed in the field of nanofluid. Numerous applications of fluids with nanostructure are found in engineering and biomedical sciences. A brief discussion of some applications of nanofluids flow in real life problems is given below.

Electronic Applications: Electronic gadgets suffer thermal challenges because of the abnormal state of heat generation and the decrease of accessible surface territory for heat expulsion. When all is said in done, there are two ways to deal with enhance the heat evacuation for electronic hardware. One is to locate an ideal geometry of cooling gadgets; another is to expand the heat transfer limit. With nanofluids, the cooling execution could be enhanced (Jang et al., 2006; Li, 2008).

Transportation: Nanofluids have incredible possibilities to enhance car performance by expanding the productivity, bringing down the weight and lessening the many-sided quality of thermal administration frameworks. Nanofluid increases the cooling rate of the system due to which more heat is removed from the high horse power engines. This technology is useful to construct more compact cooling system with lighter and smaller radiators. This in turn benefits the high performance and high fuel economy of cars and trucks. Biomedical Applications (Nano drug Delivery): To enhance the proficiency and the specificity of medication action, the framework of efficient drug delivery in few past decades was created (Li, 2008). The size of nanoparticle is very small due to which it has good solubility. Nanoparticles have novel properties that make it useful in various applications. Gold nanoparticles offer non-toxic carries for drug delivery applications. Various investigations with nanofluids have been made considering different types of nanoparticles, i.e. metal-oxides, metals and even with carbon nanotubes. In recent years, many experimentalists have examined thermal conductivity of nanofluids, considering different nanoparticles suspensions and observed the anomalous enhancement in it. Experimental studies had demonstrated the regular thermal conductivity improvement and observed the range of 15-40% over the base liquid and up gradation in the heat transfer coefficient of about 40%. Both-conductive and convective heat transfer have been explored in studies by numerous specialists

Das et al. (2003) studied thermal conductivity of water based Al_2O_3 nanofluid. Vapor combination technique was implemented to deliver nanoparticles and Ultrasonic vibrations were the mechanical mode the mode to scatter 38.4 nm estimate Al_2O_3 particles into refined water. Thermal conductivity was quantified by temperature oscillation technique. The results shows that with the addition of 1% volume fraction of Al_2O_3 nanoparticles, increase in thermal conductivity proportion was observed to be around 2% and 10.8% at 21°C and 51°C, respectively. With 4% volume fraction, the increment in accuracy in warm conductivity proportion was 9.4to 24.3% at temperature variation from 21 to 51°C. The normal rate of increment of thermal conductivity if there should be a presence of 4% volume fraction was relatively higher than that of 1% volume fraction of Al_2O_3 nanoparticles.

Mintsa et al. (2007) have experimentally demonstrated the measurement of heat capacity of water based Al_2O_3 nanofluid. Normal molecule size of 36 and 47 nm were used for the arrangement of Al2O3nanofluids. The study was performed at 3, 6 and 9% volume fractions of Al_2O_3 nanoparticles and at temperature varying from 20 to 40ºC. For the prediction of heat capacity measurement, KD2 Pro thermal analyzer was used. Results demonstrated that thermal conductivity of nanofluids expanded with temperature and volume fraction of nanoparticles. Also, at the temperature nodes of 20 and 40°C, a normal enhancement in thermal conductivity of nanofluids was approximately 16% for each kind of nanofluids (at 3, 6 and 9% volume fraction).

Li and Peterson (2007) have tested the thermal conductivity of Al_2O_3 water nanofluids utilizing steady state method. Al_2O_3 nanoparticles of size 36 nm and 47 nm were dispersed in refined water at volume fraction ranges from 0.5to 6%. Thermal conductivity of nanofluids was measured at temperature range of 27 to 37°C. It was concluded that thermal conductivity enhancement was 3% at 0.5% volume concentration. For 36 nm Al_2O_3 particles at 2% volume portion thermal conductivity upgraded from 7.7% at 27.9 °C to 18.1% at 35.0°C. Nanofluids was expanded for Al_2O_3 particles of 36 nm, at 6% volume fraction the thermal conductivity increment of nanofluids was increased from 11% at 27.5°C to 28% at 35.8°C.

From the literature reviews, there are many thermal conductivity models which depend on some assumptions. Each model has some limitations and are applied for a specific type of problem.

Maxwell Model (1873)

Maxwell studied heat conduction phenomenon analytically through suspended particles(Das et al, 2007).The Maxwell model (equation 2.1) is suitable for nm to micro sized particle with less volume concentration of particles, where the interaction between all the particles can be ignored (Vajjha and Das, 2009; Das et al., 2008). For evaluation, this model is selected here because it is a famous model (Das et al., 2007).

$$\frac{K_{nf}}{K_f} = \frac{K_p+2K_f+2(K_p-K_f)\varphi}{K_p+2K_f-(K_p-K_f)\varphi} \tag{2.1}$$

Bruggeman Model(1935)

For studing the interactions between all randomly distributed particles,the Bruggeman model was used. The homogeneous spherical inclusions for a binary mixture,this model is given by equation(2.2) (Vajjha and Das, 2009).

$$\varphi\frac{K_p-K_{nf}}{K_p+2K_{nf}} + (1-\varphi)\frac{K_p-K_{nf}}{K_p+2K_{nf}} = 0 \tag{2.2}$$

Hamilton-Crosser Model (1962)

For measuring the thermal conductivity of particle-fluid mixture, the Hamilton –Crosser model was used. Hamilton-Crosser model is depends on the sphericity of particles, thermal conductivity of fluid and particles, volume fraction. Sphericity is 1 for the spherical particle. Hamilton-Crosser equation is similar to the Maxwell's equation (Zhang et al., 2007). This model is given by equation (2.3). For measuring the thermal conductivity of any shape of particle, this model was used (Yu et al., 2007).

$$\frac{K_{nf}}{K_f} = \frac{K_p+(n'-1)K_f-(n'-1)\varphi(K_f-K_p)}{K_p+(n'-1)K_f+\varphi(K_f-K_p)} \tag{2.3}$$

Where, $n' = \frac{3}{\Psi}$

Jeffrey Model (1973)

The heat conduction through stationary, homogenous and random suspension of spherical shape particles in constant conductivity matrix is investigated by Jeffery (1073).The model is given by equation 2.4. Jeffrey model was found appropriate for spherical shaped particles. The model is suitable for low volume fraction of particles (Jeffrey, 1973).

$$\frac{K_{nf}}{K_f} = 1 + 3\varphi\beta + \varphi^2\left\{3\beta^2 + \frac{3\beta^3}{4}\right\} \tag{2.4}$$

Yu and Choi Model (2003)

Yu and Choi model was developed by modifying the Maxwell model. By taking the effect of liquid nano-layer around the nanoparticles for the thermal conductivity of nanofluids.
When the size of nanoparticles is less than 10nm, the thermal conductivity of nanofluid is influenced by nano-layer (Yu and Choi, 2003). In this thesis, for calculation the value of nano-layer is used 1nm (as employed by Yu and Choi, 2003; Xie et al., 2005; Murshed et al., 2008)

$$\frac{K_{nf}}{K_f} = \frac{K_p + 2K_f + 2(K_p - K_f)\varphi(1+\gamma)^3}{K_p + 2K_f - (K_p - K_f)\varphi(1+\gamma)^3} \tag{2.5}$$

Koo and Kleinstreuer Model (2004)

For the effective thermal conductivity of nano fluid, this model measured the thermal conductivity of nanofluid with the effect of both conventional static part and Brownian motion.There were two types of model, that include Brownian motion of particles, as given by equation (2.7) (version 1) and (2.8) (version 2).

$$K_{nf} = K_{static} + K_{Brownian}$$

$$K_{Brownian} = 37.5^2 * 75\sqrt{\frac{18}{\pi}}p\Psi\varphi\rho_p C_p\sqrt{\left(\frac{K_B}{\rho_P}\right)}\sqrt{\frac{T}{d}}\sqrt{\frac{L}{d}}f(T,\varphi) \tag{2.6}$$

$$K_{Brownian} = 5 * 10^4\Psi\varphi\rho_l C_l\sqrt{\left(\frac{K_B}{\rho_P}\right)}\sqrt{\frac{T}{d}}f(T,\varphi) \tag{2.7}$$

Where, $\frac{L}{d} = 1$

$$f(T, \varphi) = (-6.04\varphi + 0.4705)T + (1722.3\varphi - 134.63) \quad (2.8)$$

For Al_2O_3-H_2O nanofluids and ϕ> 1%, $\Psi = 0.0017(100\varphi)^{-0.0841}$

Expectation value of particles to move in one direction (p) is 0.197 (Koo, 2004). $f(T, \varphi)$is valid for $1\% < \varphi < 4\%$ and 300<T<325K.

Xie et al. Model (2005)

This model is based on volume fraction, Nano layer thickness at fluid-particle interface, thermal conductivity of fluid and particle and particle size. This model was developed by taking the effect of interfacial nanolayer at the liquid-solid interface. For low volume fraction of nanoparticle (Xie et al., 2005), this model is used. The model equation is given by equation (2.9). For calculation, the value of nano layer is taken 1 nm (Yu and Choi, 2003; Xie et al., 2005; Murshed et al., 2008).

$$\frac{K_{nf} - K_f}{K_f} = 3\Theta\varphi_T + \frac{3\Theta^2\varphi_T{}^2}{1 - \Theta\varphi_T} \quad (2.9)$$

Where, $= \frac{B_{ij}\left[(1+\gamma)^3 - \frac{B_{pl}}{B_{fl}}\right]}{(1+\gamma)^3 + 2B_{pl}B_{lf}}$; $B_{pl} = \frac{K_p - K_l}{K_p + 2K_l}$; $B_{fl} = \frac{K_f - K_l}{K_f + 2K_l}$; $B_{lf} = \frac{K_l - K_f}{K_l + 2K_f}$

$K_l = \frac{K_f M^2}{(M-\gamma)\ln(1+M) + \gamma M}$, $\varphi_T = \varphi(1+\gamma)^3$, $\gamma = \frac{\delta}{r_p}$, $M = \alpha(1+\gamma) - 1$

Murshed et al. Model (2008)

This model is based on volume fraction, Nano layer thickness at fluid-particle interface, thermal conductivity of fluid and particle and particle size. This model was developed by taking the effect of interfacial nanolayer at the liquid-solid interface**.** There is a uniform heat flux between all stationary nanoparticles. The effective thermal conductivity equations are given by equation (2.10) and (2.11).For the calculation purpose, the value of interfacial layer thickness is used 1nm (Murshed et al., 2008).Also, K_{lr} is used 3 K_f in equation 2.10 and 2.11 (as employed by Murshed et al., 2008)**.**

$$K_{nf} = \frac{(K_p - K_{lr})\varphi_p K_{lr}(2{\varepsilon_1}^3 - \varepsilon^3 + 1) + (K_p + 2K_{lr}){\varepsilon_1}^3\{\varphi_p \varepsilon^3 (K_{lr} - K_f) + K_f\}}{(K_p + 2K_{lr}){\varepsilon_1}^3 - (K_p - K_{lr})\varphi_p({\varepsilon_1}^3 - \varepsilon^3 + 1)} \quad (2.10)$$

$$K_{nf} = \frac{(K_p - K_{lr})\varphi_p K_{lr}({\varepsilon_1}^2 - \varepsilon^2 + 1) + (K_p + K_{lr}){\varepsilon_1}^2\{\varphi_p \varepsilon^2 (K_{lr} - K_f) + K_f\}}{(K_p + K_{lr}){\varepsilon_1}^2 - (K_p - K_{lr})\varphi_p(\varepsilon_1 + \varepsilon_2 - 1)} \quad (2.11)$$

Where, $\varepsilon = 1 + \frac{\delta}{r}$; $\varepsilon_1 = 1 + \frac{\delta}{2r}$

Chon et al. Model (2005)

Buckingham π theorem was used to develop this empirical model. The experimental results with linear regression analysis R^2 value of 95% was shown by Chon et al., 2005. For experiments the size of nanoparticles were considered 11,150 and 47 nm. For this experiment volume fraction 1% and 4% was used. The temperature range of 21°C to 71°C was used (Chon et al., 2005).

$$\frac{K_{nf}}{K_f} = 1 + 64.7\varphi^{0.746}\left(\frac{d_f}{d_p}\right)^{0.369}\left(\frac{K_p}{K_f}\right)^{0.7476} Pr^{0.9955}\, Re^{1.2321} \quad (2.12)$$

Where; $Re = \frac{\rho_f T K_B}{3\pi\mu^2 l_F}$, $Pr = \frac{\mu C_f}{K_f}$, $l_f = \frac{1}{\pi {d^2}_f \sqrt{2\mu}}$,

Pak and Cho (1998) observed turbulent friction and heat transfer of nanofluids in round pipe due to presence of alumina and titanium oxide. They founded that the Nusselt number of the nanofluids had a direct relationship with volume fraction of the suspended nanoparticle, and Reynolds number. An expansion in thermal conductivity of the additional nanoparticles may incorporate molecule agglomeration. Brownian motion(Jang et al., 2006; Chon et al., 2005), thermophoresis, nanoparticle size(Chon et al., 1995; Prasher et al. 2005); molecule shape/surface area (Yu et al., 1999; Keblinski et al., 2005), liquid layering on the nanoparticle-fluid interface (Yu et al., 1999; Leong et al., 2006; Murshed et al., 2008), Temperature(Chon et al., 2005; Koo et al., 2005; Koo et al., 2004).

Sheikholeslami et al. (2013) have studied the two phase simulation of heat transfer and Nano-fluid flow utilizing heat line investigation. In their study they used control volume base Finite element method to solve the heat transfer issues of enclosure filled with nanofluid of heat. They have used the concept of Brownian motion and thermophoresis in the model of Nanofluid. Heat line visualization is incorporated to understand the isotherm pattern to study the in the heat transfer between cold and hot region. They examine the effect of Ra number, buoyancy ratio number, Lewis number on streamlines, isotherm and headline. The result shows that the reduction in Nu number brings increment in the buoyancy number.

Bourants et al. (2014) have studied the heat transfer and natural convection of nanofluids in a porous media. In this study they investigated natural convection of nanofluid in a square cavity filled with porous matrix, for this purpose they use a mesh-less technique. To determine the thermal conductivity of Nanofluid, alternative expressions were suggested. Excellent agreement of experimental data with numerical data was found.

Oztop et al. (2008) have studied the numerical formulation of free convection in a partially heated rectangular shaped enclosures filled with nanofluid. In this studied they used a flush mounted heater of a finite length which is located to the left vertical wall. There is a temperature difference between left and right wall. The finite volume technique is used for solving the governing equations. The result shows that mean Nusselt value increases with volume fraction. Heat transfer is also increased with the height of heater. The investigation showed that heat transfer is enhanced with low aspect ratio.

Kamyar et al. (2012) have presented a research paper on application of computational fluid dynamics on nanofluids. They said that with the help of some slip mechanisms such as thermophoresis that lead to the increase in heat transfer, solving a two-phase model for nanofluids has become easier. Two phase model gives accurate results compared to the single phase approach. They suggested that by considering the effect of Brownian motion and temperature dependency of viscosity and thermal conductivity accuracy of ther results can be enhanced.

In 2006, Buongiorno based at MIT, gave a surprising review on convective transport in nanofluids. He built two-phase non-homogeneous model that can create a relative speed between the base liquid and the nanoparticles incorporating seven slip systems. Of these

systems, just Brownian diffusion and thermophoresis were observed to be critical without turbulent impacts.

The above writing manages nanofluids as Newtonian liquids. Non-Newtonian rheological conduct of nanofluids was shown by numerous analysts:

Recently, (Khan and Gorla, 2011) conducted heat transfer analysis in non-Newtonian nanofluids on a non-isothermal stretching wall. Since, the elastic behavior is inherent in non-Newtonian fluids various uses of viscoelastic liquids in a few mechanical assembling forms have prompted restored enthusiasm among scientists to explore viscoelastic boundary layer stream over an extending plastic sheet(Dandapat and Gupta, 1989), (Rajagopal et al., 1984) ; (Rajagopal et al., 1987) and (Rao , 1996).

Flow, mass transfer and heat in porous media is a common phenomenon in nature and in many fields of science and engineering. The most common examples includes transport of water in trees and plants and fertilizers or wastes in soil, heated underground electrical cables, nuclear waste repository and oil recovery processes. Nield and Kuznetsov (2009) examined the porous medium saturated by nanofluids and investigated the Cheng-Minkowycz problem for free convection boundary-layer flow. Various investigations in literature had been carried out on heat convection in nanofluids saturated by porous media (Ferdows et al., 2012; Gorla et al., 2011).

Chapter 3

Numerical Investigation into Performance of Nanofluid

3.1 Mathematical analysis of heat transfer enhancement along a vertical plate using nanofluid.

In the present work the equations are formulated by using models of thermal conductivity.

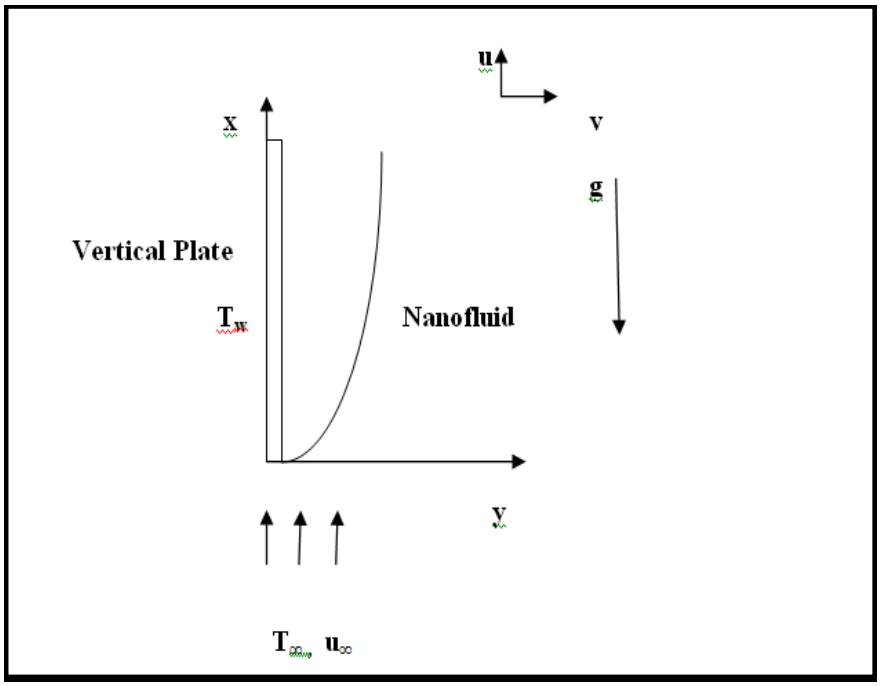

Figure 3.1: Geometry and co-ordinate system

In the present work the flow along the vertical plate has been considered along the vertical plate in order to enhance heat transfer from the plate. The geometry is shown in Figure 3.1. The following assumptions have been made for modeling such flow.

In writing the equations (3.1) to (3.3), following assumptions were taken:

1. Steady state, two-dimensional, incompressible, laminar flow of nanofluid over a vertical, semi-infinite flat plate.

2. Flow along x direction (vertical flow)

3. Steady temperature profile along plate.

4. Plate temperature is higher than ambient temperature.

5. Thermal equilibrium between nanoparticles and working fluid.

6. No-slip condition between particle and fluid.

The flow mechanism is characterized by steady conservation of mass, momentum and thermal energy equations for nanofluids can be composed in Cartesian directions x and y as.

$$\frac{\partial u}{\partial x} + \frac{\partial v}{\partial y} = 0 \tag{3.1}$$

$$u\frac{\partial u}{\partial x} + v\frac{\partial u}{\partial y} = \frac{1}{\rho_{nf}}\left[\mu_{nf}\frac{\partial^2 u}{\partial y^2} + (\rho\beta)_{nf}\, g(T - T_\infty)\right] \tag{3.2}$$

$$u\frac{\partial T}{\partial x} + v\frac{\partial T}{\partial y} = \frac{1}{(\rho C_p)_{nf}}\left[k_{nf}\frac{\partial^2 T}{\partial y^2} + Q_0(T - T_\infty)\right] \tag{3.3}$$

Subject to the boundary conditions −

X = 0, y > 0 , $T = T_\infty$, $u = u_\infty$

X > 0, y = 0 , $T = T_w$, u = 0, v = 0

For nanofluid, introducing the expression for ρ_{nf} , $(\rho\beta)_{nf}$ and $(\rho C_P)_{nf}$

$$\rho_{nf} = (1 - \varphi)\rho_f + \varphi\rho_s \tag{3.4}$$

$$(\rho\beta)_{nf} = (1 - \varphi)(\rho\beta)_f + \varphi(\rho\beta)_s \tag{3.5}$$

$$(\rho C_p)_{nf} = (1 - \varphi)(\rho C_p)_f + \varphi(\rho C_p)_s \tag{3.6}$$

$$\mu_{nf} = \frac{\mu_f}{(1-\varphi)^{2.5}} \tag{3.7}$$

$$\frac{K_{nf}}{K_f} = \frac{K_p + 2K_f + 2(K_p - K_f)\varphi}{K_p + 2K_f - (K_p - K_f)\varphi} \tag{3.8}$$

3.2 Non-dimensionlisation of the equation

x and y co-ordinate is converted into $\boldsymbol{\xi}$ and $\boldsymbol{\eta}$ natural co-ordinate .

Substituting the following dimensionless variables:

$$\xi = \frac{x}{L} \tag{3.9}$$

$$\psi(x, y) = (v_f u_\infty x)^{1/2} f(\xi, \eta) \tag{3.10}$$

$$\eta = y\left(\frac{u_\infty}{v_f x}\right)^{1/2} \tag{3.11}$$

$$\theta(\eta) = \frac{T - T_\infty}{T_w - T_\infty} \tag{3.12}$$

$\psi(x, y)$ is the stream function

$u = \frac{\partial \psi}{\partial y}$ and $v = -\frac{\partial \psi}{\partial x}$

In terms of these variables the velocity components can be expressed as-

$$u = u_\infty f' \tag{3.13}$$

$$v = -\left(\frac{\upsilon u_\infty}{x}\right)^{1/2}\left\{\frac{1}{2}f + \xi\frac{\partial f}{\partial \xi} - \frac{\eta}{2}f'\right\} \tag{3.14}$$

Converting momentum equation (3.2) into non-dimensionless variables-

$$u\frac{\partial u}{\partial x} + v\frac{\partial u}{\partial y} = \frac{1}{\rho_{nf}}\left[\mu_{nf}\frac{\partial^2 u}{\partial y^2} + (\rho\beta)_{nf}\, g(T - T_\infty)\right]$$

$$\frac{\partial u}{\partial x} = \frac{\partial u}{\partial \xi} * \frac{\partial \xi}{\partial x}$$

$$\frac{\partial u}{\partial x} = u_\infty \frac{\partial f'}{\partial \xi} * \frac{1}{L}$$

$$\frac{\partial u}{\partial y} = \frac{\partial u}{\partial \eta} * \frac{\partial \eta}{\partial y}$$

$$\frac{\partial u}{\partial y} = u_\infty \frac{\partial f'}{\partial \eta}\left[\frac{u_\infty}{\upsilon_f x}\right]^{1/2}$$

$$\frac{\partial f'}{\partial \eta} = f''$$

L.H.S-

$${u_\infty}^2\left[\frac{1}{L}f'\frac{\partial f'}{\partial \xi} - \frac{1}{\xi L}\left\{\frac{1}{2}ff'' + \xi f''\frac{\partial f}{\partial \xi} - \frac{\eta}{2}f'f''\right\}\right]$$

$f'f''$ is a very small quantity so we can neglect this term

$${u_\infty}^2\left[\frac{1}{L}f'\frac{\partial f'}{\partial \xi} - \frac{1}{\xi L}\left\{\frac{1}{2}ff'' + \xi f''\frac{\partial f}{\partial \xi}\right\}\right] \tag{3.15}$$

R.H.S-

$$\frac{\partial^2 u}{\partial y^2} = u_\infty \frac{\partial^2 f'}{\partial y^2}$$

$$\frac{\partial^2 f'}{\partial y^2} = \frac{\partial}{\partial y}\left(\frac{\partial f'}{\partial y}\right) = \frac{\partial}{\partial y}\left(\frac{\partial f'}{\partial \eta} * \frac{\partial \eta}{\partial y}\right) = \frac{u_\infty}{\upsilon_f x}f'''$$

$$\frac{\partial^2 u}{\partial y^2} = \frac{{u_\infty}^2}{\upsilon_f \xi L}f'''$$

$$R_i = \frac{G_r}{{R_e}^2} = \frac{g\beta(T_w - T_\infty)L}{{u_\infty}^2}$$

$$\frac{1}{\left(1-\varphi+\varphi\frac{\rho_s}{\rho_f}\right)\xi L}\left[\frac{{u_\infty}^2}{(1-\varphi)^{2.5}}f''' + \left(1 - \varphi + \varphi\frac{(\rho\beta)_s}{(\rho\beta)_f}\right){u_\infty}^2\xi\theta R_i\right] \tag{3.16}$$

L.H.S (3.15) = R.H.S (3.16)

$$\frac{1}{\left(1-\varphi+\varphi\frac{\rho_S}{\rho_f}\right)}\left[\frac{1}{(1-\varphi)^{2.5}}f'''+\left(1-\varphi+\varphi\frac{(\rho\beta)_s}{(\rho\beta)_f}\right)\xi\theta R_i\right]+\frac{1}{2}ff'=\xi\left(f'\frac{\partial f'}{\partial\xi}-f''\frac{\partial f}{\partial\xi}\right) \quad (3.17)$$

Converting energy equation (3.3) into non-dimensionless variables-

$$u\frac{\partial T}{\partial x}+v\frac{\partial T}{\partial y}=\frac{1}{(\rho C_p)_{nf}}\left[k_{nf}\frac{\partial^2 T}{\partial y^2}+Q_0(T-T_\infty)\right]$$

$$\theta=\frac{T-T_\infty}{T_w-T_\infty}$$

$$\theta=\frac{T}{(T_w-T_\infty)}-\frac{T_\infty}{(T_w-T_\infty)}$$

$\frac{T_\infty}{(T_w-T_\infty)}$ is negligible because $T_w \gg T_\infty$

$$\theta=\frac{T}{(T_w-T_\infty)}$$

$$\frac{\partial T}{\partial x}=(T_w-T_\infty)\frac{\partial\theta}{\partial x}=(T_w-T_\infty)\frac{\partial\theta}{\partial\xi}*\frac{\partial\xi}{\partial x}=(T_w-T_\infty)\frac{\partial\theta}{\partial\xi}*\frac{1}{\mathrm{L}}$$

$$\frac{\partial T}{\partial y}=(T_w-T_\infty)\frac{\partial\theta}{\partial y}=(T_w-T_\infty)\frac{\partial\theta}{\partial\eta}*\frac{\partial\eta}{\partial y}=(T_w-T_\infty)\theta'\left[\frac{u_\infty}{\upsilon_f x}\right]^{1/2}$$

L.H.S-

$$\frac{u_\infty}{L}(T_w-T_\infty)\left[f'\frac{\partial\theta}{\partial\xi}-\frac{1}{\xi}\left\{\frac{1}{2}f\theta'+\xi\theta'\frac{\partial f}{\partial\xi}\right\}\right] \quad (3.18)$$

R.H.S-

$$\frac{\partial^2 T}{\partial y^2}=\frac{\partial}{\partial y}\left(\frac{\partial T}{\partial y}\right)=(T_w-T_\infty)\frac{u_\infty}{\upsilon_f x}\theta''$$

$$Q=\frac{Q_0 x}{u_\infty(\rho C_p)_f}$$

$$P_r=\frac{\mu C_p}{k}$$

$$\frac{(T_w-T_\infty)u_\infty}{\xi L}\left[\frac{1}{\left(1-\varphi+\varphi\frac{(\rho C_p)_S}{(\rho C_p)_f}\right)}\left\{\frac{1}{P_r}\left(\frac{k_{nf}}{k_f}\right)\theta''+Q\theta\right\}\right] \quad (3.19)$$

L.H.S (3.18) =R.H.S (3.19)

$$\frac{1}{\left(1-\varphi+\varphi\frac{(\rho C_p)_S}{(\rho C_p)_f}\right)}\left\{\frac{1}{P_r}\left(\frac{k_{nf}}{k_f}\right)\theta''+Q\theta\right\}+\frac{1}{2}f\theta'=\xi\left[f'\frac{\partial\theta}{\partial\xi}-\theta'\frac{\partial f}{\partial\xi}\right] \quad (3.20)$$

Equations (3.17) & (3.20) are the final non-dimensionless mass momentum and energy equation.

3.3 Transformation of the boundary conditions

X = 0, y > 0 , T = T_∞ , u = u_∞

X > 0, y = 0 , T = T_w, u = 0, v = 0

$$u = u_\infty f'$$

$$v = -\left(\frac{v u_\infty}{x}\right)^{1/2}\left\{\frac{1}{2}f + \xi\frac{\partial f}{\partial \xi} - \frac{\eta}{2}f'\right\}$$

$$\xi = \frac{x}{L}$$

$$\eta = y\left(\frac{u_\infty}{v_f x}\right)^{1/2}$$

$$\theta(\eta) = \frac{T - T_\infty}{T_w - T_\infty}$$

Transformed boundary Conditions-

$$\theta(\xi, 0) = 1 \quad , \quad f'(\xi, 0) = 0$$

$$\theta(\xi, \infty) = 0 \quad , \quad f'(\xi, \infty) = 1$$

$$f(\xi, 0) + 2\xi\frac{\partial f}{\partial \xi} = 0$$

3.4 Method of solution

The arrangement of partial differential equations given by (3.17) and (3.20) are profoundly non-linear, in this manner, can't be illuminated analytically. The vibrational finite element technique has been actualized.

3.4.1 Finite element method

- The FEM is a most versatile technique to solve partial difference equations. FEM the entire space is isolated into littler components of finite dimensions.
- Finite element discretization - In finite element discretization we change over the entire area into sub space. Each sub area is called component and gathering of all component is called mesh.

3.4.2 Generation of the element equation

- A component is secluded from the mesh and the vibrational detailing of the given issue over the component is developed.
- The element equations are made by substituting a rough arrangement of the vibrational issue.
- For constructing element stiffness matrix we are utilizing the component interpolation function.

3.4.3 Grouping of Element Equations

The acquired mathematical equations are assembled by forcing the inter element continuity conditions.

3.4.4 Imposition of boundary conditions

The basic and characteristic boundary conditions are imposed on the assembled equations.

3.4.5 Solution of assembled equation

The final assembled equations can be solved by Gauss elimination method, LU decomposition method, etc.

ASSUME-

$$h = f' \tag{3.21}$$

Now the equation (3.6) and (3.9) is reduced by using 'h' in place of 'f''

$$\frac{1}{\left(1-\varphi+\varphi\frac{\rho_s}{\rho_f}\right)}\left[\frac{1}{(1-\varphi)^{2.5}}h'' + \left(1-\varphi+\varphi\frac{(\rho\beta)_s}{(\rho\beta)_f}\right)\xi\theta R_i\right] + \frac{1}{2}fh' = \xi\left(h\frac{\partial h}{\partial\xi} - h'\frac{\partial f}{\partial\xi}\right) \tag{3.22}$$

$$\frac{1}{\left(1-\varphi+\varphi\frac{(\rho C_p)_s}{(\rho C_p)_f}\right)}\left\{\frac{1}{P_r}\left(\frac{k_{nf}}{k_f}\right)\theta'' + Q\theta\right\} + \frac{1}{2}\mathrm{f}\theta' = \xi\left[h\frac{\partial\theta}{\partial\xi} - \theta'\frac{\partial f}{\partial\xi}\right] \tag{3.23}$$

3.4.6 The corresponding boundary conditions become

$$\theta(\xi,0) = 1 \quad , \quad h(\xi,0) = 0 \tag{3.24}$$

$$\theta(\xi,\infty) = 0 \quad , \quad h(\xi,\infty) = 1 \tag{3.25}$$

$$f(\xi,0)+2\xi\frac{\partial f}{\partial \xi}=0 \tag{3.26}$$

3.4.7 Variational formulation

$$\int w_1\left\{\frac{\partial f}{\partial \eta}-h\right\}d\xi d\eta=0 \tag{3.27}$$

$$\int w_2\left\{\frac{1}{\left(1-\varphi+\varphi\frac{\rho_s}{\rho_f}\right)}\left[\frac{1}{(1-\varphi)^{2.5}}h''+\left(1-\varphi+\varphi\frac{(\rho\beta)_s}{(\rho\beta)_f}\right)\xi\theta R_i\right]+\frac{1}{2}fh'-\xi\left(h\frac{\partial h}{\partial \xi}-h'\frac{\partial f}{\partial \xi}\right)\right\}d\xi d\eta=0 \tag{3.28}$$

$$\int w_3\left\{\frac{1}{\left(1-\varphi+\varphi\frac{(\rho C_p)_s}{(\rho C_p)_f}\right)}\left\{\frac{1}{P_r}\left(\frac{k_{nf}}{k_f}\right)\theta''+Q\theta\right\}+\frac{1}{2}f\theta'-\xi\left[h\frac{\partial\theta}{\partial\xi}-\theta'\frac{\partial f}{\partial\xi}\right]\right\}d\xi d\eta=0 \tag{3.29}$$

Where w1, w2, w3 are arbitrary test function and might be seen as the variety in f, h and θ, individually.

Finite element formulation

$$\begin{aligned} f&=\textstyle\sum_{j=1}^{4} f_j\,\psi_j \\ h&=\textstyle\sum_{j=1}^{4} h_j\psi_j \\ \theta&=\textstyle\sum_{j=1}^{4}\theta_j\psi_j \end{aligned} \tag{3.30}$$

Where ψ_1, $\psi 2$, $\psi 3$, ψ_4 are the linear interpolation functions for a rectangular component as appeared in Figure 3.2.

$$\psi_1=\frac{(\xi_{e+1}-\xi)(\eta_{e+1}-\eta)}{(\xi_{e+1}-\xi_e)(\eta_{e+1}-\eta_e)}$$

$$\psi_2=\frac{(\xi-\xi_e)(\eta_{e+1}-\eta)}{(\xi_{e+1}-\xi_e)(\eta_{e+1}-\eta_e)} \tag{3.31}$$

$$\psi_3 = \frac{(\xi-\xi_e)(\eta-\eta_e)}{(\xi_{e+1}-\xi_e)(\eta_{e+1}-\eta_e)}$$

$$\psi_4 = \frac{(\xi_{e+1}-\xi)(\eta-\eta_e)}{(\xi_{e+1}-\xi_e)(\eta_{e+1}-\eta_e)}$$

The finite element model equation-

$$\begin{bmatrix} K^{11} & K^{12} & K^{13} \\ K^{21} & K^{22} & k^{23} \\ K^{31} & K^{32} & K^{33} \end{bmatrix} \begin{bmatrix} f \\ h \\ \theta \end{bmatrix} = \begin{bmatrix} b^1 \\ b^2 \\ b^3 \end{bmatrix}$$

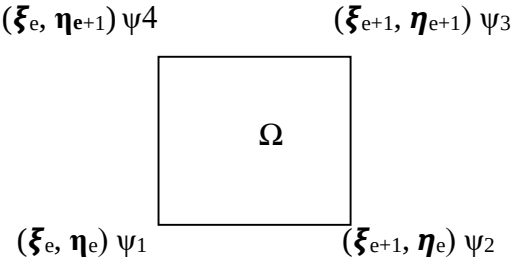

Figure 3.2: Rectangular finite element

The element model equation has formed by Green lamina theorem
Where $[K^{mn}]$ and $[b^m]$ (m, n = 1, 2, 3) are characterized as:

$$k_{ij}^{11} = \int \psi_i \frac{\partial \psi_j}{\partial \eta} d\xi \, d\eta,$$

$$k_{ij}^{12} = -\int \psi_i \psi_j \, d\xi \, d\eta,$$

$$k_{ij}^{13} = 0,$$

$$k_{ij}^{21} = \int \left\{ \psi_i \xi \frac{\partial \bar{h}}{\partial \eta} \frac{\partial \psi_j}{\partial \eta} + \psi_i \psi_j \frac{\partial \bar{h}}{\partial \eta} \right\} d\xi d\eta,$$

$$k_{ij}^{22} = -\frac{1}{\left(1-\varphi+\varphi\frac{\rho_s}{\rho_f}\right)} \frac{1}{(1-\varphi)^{2.5}} \int \frac{\partial \psi_i}{\partial \eta} \frac{\partial \psi_j}{\partial \eta} \, d\xi d\eta - \int \psi_i \xi \frac{\partial \bar{h}}{\partial \xi} \frac{\partial \psi_i}{\partial \eta} d\xi \, d\eta,$$

$$k_{ij}^{23} = Ri \int \psi_i \xi \, \psi_j d\xi d\eta,$$

$$k_{ij}^{31} = \int \psi_i \frac{\partial \psi_j}{\partial \eta} \bar{\theta} d\xi \, d\eta,$$

$$k_{ij}^{32} = \int \psi_i \psi_j \frac{\partial \bar{\theta}}{\partial \xi} d\xi \, d\eta,$$

$$k_{ij}^{33} = \frac{1}{\left(1-\varphi+\varphi\frac{(\rho c_p)_s}{(\rho c_p)_f}\right)} \left(\frac{1}{P_r} \left(\frac{k_{nf}}{k_f} \right) \int \frac{\partial \psi_i}{\partial \eta} \frac{\partial \psi_j}{\partial \eta} \, d\xi d\eta + Q \int \psi_i \psi_j d\xi \, d\eta \right) - \frac{1}{2} \int \psi_i \bar{F} \frac{\partial \psi_j}{\partial \eta} d\xi d\eta,$$

$$b_i^1 = 0,$$

$$b_i^2 = -\frac{1}{\left(1-\varphi+\varphi\frac{\rho_s}{\rho_f}\right)}\frac{1}{(1-\varphi)^{2.5}}\oint \psi_i q_{n2} ds,$$

$$b_i^3 = -\frac{1}{P_r}\frac{1}{\left(1-\varphi+\varphi\frac{(\rho C_p)_s}{(\rho C_p)_f}\right)}\left(\frac{k_{nf}}{k_f}\right)\oint \psi_i q_{n3} ds,$$

Where

$$\bar{h} = \sum_{i=1}^{4} \bar{h_i}\,\psi_i,$$

$$\bar{f} = \sum_{i=1}^{4} \bar{f_i}\,\psi_i,$$

$$\bar{\theta} = \sum_{i=1}^{4} \bar{\theta_i}\,\psi_i,$$

$$\frac{\partial \bar{h}}{\partial \eta} = \sum_{i=1}^{4} \bar{h_i}\frac{\partial \psi_i}{\partial \eta},$$

$$\frac{\partial \bar{h}}{\partial \xi} = \sum_{i=1}^{4} \bar{h_i}\frac{\partial \psi_i}{\partial \xi},$$

$$\frac{\partial \bar{\theta}}{\partial \xi} = \sum_{i=1}^{4} \bar{h_i}\frac{\partial \psi_i}{\partial \xi},$$

Based upon the mathematical model used for the flow of nanofluid across flat vertical plate, the numerical solution is obtained using finite element method in order to determine the variation of temperature across the length of plate. To determine the boundary value of the problem, the appropriate value of $\boldsymbol{\eta}_{\max}$ (range of the domain) and $\boldsymbol{\xi}_{\max}$ (range of the vertical plate) is used which satisfied all the boundary conditions and give a good result for the numerical problem. For the numerical solution some governing parameters are used such as Ri (Richardson number), Pr (Prandtle number). Richardson number is a method of measuring the effect of buoyancy forces with respect to inertia effects of the external forced or free stream flow on the heat and fluid flow. The impact of forced convection prevails for Ri=0 and vice versa for Ri =∞. Prandtl number is the dimensionless number. Thermal diffusivity dominants for smaller values of Prandtl number, Pr << 1 whereas for Pr >> 1, momentum diffusivity dominates. In all such cases, default estimation of the governing parameters are: Ri=1, Q=0.05, Pr=6.2 Cu nanoparticles, unless generally expressed. The effect of nanofluid (water based having 4% Cu nanoparticles) on the dimensionless temperature profile is also shown in the graphs.

Table 3.1: Thermo physical properties of water and nanoparticle

	ρ (kg m^{-3})	C_p ($Jkg^{-1}k^{-1}$)	k (Wm^{-1} k^{-1})	β *10^{-5}(k^{-1})
H_2O	`1000	4179	0.613	21
Al_2O_3	3970	765	40	0.85
Cu	8933	385	401	1.67

For this numerical study Cu nanoparticles were used with volume fraction 4%. The flow is considered only in upward direction so the degree of freedom is 1. Nine elements equation were obtained by green lamina theorem (Appendix A). Due to one degree of freedom, there are sixteen nodes. The flow region is divided into 9 rectangular elements of equal size. The whole domain is mainly divided into 16 nodes since there are 9 elements and each element has four nodes. Hence the global matrix was calculated for sixteen nodes similarly element matrix was generated for each element.

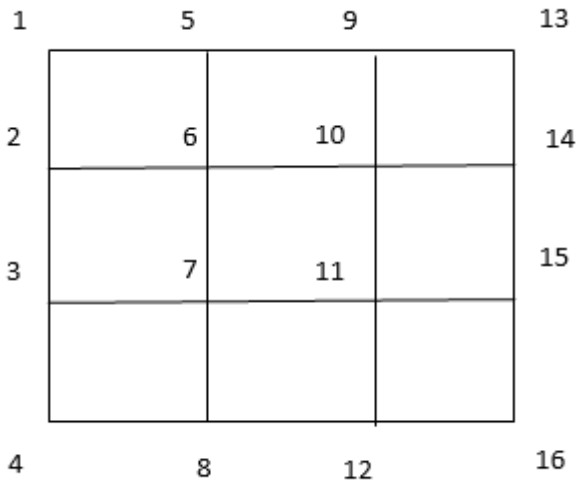

Figure 3.3: Nodal presentation of the problem

Calculate element stiffness matrix for each element after that generate global stiffness matrix for sixteen nodes which are provided as following:

$$K^{11} = \begin{matrix} \\ 2 \\ 6 \\ 5 \\ 1 \end{matrix} \begin{matrix} \begin{matrix} 2 & 6 & 5 & 1 \end{matrix} \\ \begin{bmatrix} -0.333 & -0.166 & 0.166 & 0.333 \\ -0.166 & -0.333 & 0.333 & 0.166 \\ 0.166 & 0.333 & 0.333 & 0.166 \\ 0.333 & 0.166 & 0.166 & 0.333 \end{bmatrix} \end{matrix}$$

$$K^{12} = \begin{matrix} \\ -0.44 \\ -0.22 \\ -0.11 \\ -0.22 \end{matrix} \begin{matrix} 6 \\ -0.22 \\ -0.44 \\ -0.22 \\ -0.11 \end{matrix} \begin{matrix} 10 \\ -0.11 \\ -0.22 \\ -0.44 \\ -0.22 \end{matrix} \begin{matrix} 9 \\ -0.22 \\ -0.11 \\ -0.22 \\ -0.44 \end{matrix} \begin{matrix} 5 \\ \\ \\ \\ \end{matrix}$$

$$K^{13} = \begin{matrix} \\ 0 \\ 0 \\ 0 \\ 0 \end{matrix} \begin{matrix} 10 \\ 0 \\ 0 \\ 0 \\ 0 \end{matrix} \begin{matrix} 14 \\ 0 \\ 0 \\ 0 \\ 0 \end{matrix} \begin{matrix} 13 \\ 0 \\ 0 \\ 0 \\ 0 \end{matrix} \begin{matrix} 9 \\ 0 \\ 0 \\ 0 \\ 0 \end{matrix}$$

$$K^{21} = \begin{matrix} \\ -0.22 \\ 0 \\ 0.00 \\ -0.11 \end{matrix} \begin{matrix} 3 \\ 0.0 \\ -0.22 \\ -0.11 \\ 0.0 \end{matrix} \begin{matrix} 7 \\ 0 \\ -0.11 \\ 0.220 \\ 0.0 \end{matrix} \begin{matrix} 6 \\ -0.11 \\ 0 \\ 0 \\ 0.22 \end{matrix} \begin{matrix} 2 \\ \\ \\ \\ \end{matrix}$$

$$K^{22} = \begin{matrix} \\ -0.224 \\ -0.14 \\ 0.14 \\ 0.224 \end{matrix} \begin{matrix} 7 \\ -0.14 \\ -0.22 \\ 0.224 \\ 0.14 \end{matrix} \begin{matrix} 11 \\ -0.14 \\ 0.224 \\ -0.335 \\ -0.14 \end{matrix} \begin{matrix} 10 \\ 0.14 \\ 0.14 \\ -0.14 \\ -0.335 \end{matrix} \begin{matrix} 6 \\ \\ \\ \\ \end{matrix}$$

$$K^{23} = \begin{matrix} \\ -0.22 \\ 0 \\ 0 \\ -0.11 \end{matrix} \begin{matrix} 11 \\ 0 \\ 0.22 \\ 0.11 \\ 0 \end{matrix} \begin{matrix} 15 \\ 0 \\ 0.11 \\ 0.22 \\ 0 \end{matrix} \begin{matrix} 14 \\ 0 \\ 0.11 \\ 0 \\ -0.22 \end{matrix} \begin{matrix} 10 \\ -0.11 \\ 0 \\ 0 \\ \end{matrix}$$

$$\begin{matrix} 4 & 8 & 7 & 3 \end{matrix}$$

$$K^{31} = \begin{bmatrix} -0.16 & -0.055 & 0.055 & 0.166 \\ -0.055 & -0.166 & 0.166 & 0.055 \\ 0.055 & 0.166 & 0.166 & 0.055 \\ 0.166 & 0.055 & 0.055 & 0.166 \end{bmatrix}$$

$$K^{32} = \begin{array}{c} \begin{matrix} 8 & 12 & 11 & 7 \end{matrix} \\ \begin{bmatrix} -0.166 & -0.083 & -0.027 & -0.055 \\ -0.083 & 0.16 & 0.055 & 0.027 \\ -0.027 & 0.055 & 0.166 & 0.083 \\ -0.055 & 0.027 & 0.083 & -0.166 \end{bmatrix} \end{array}$$

$$K^{33} = \begin{array}{c} \begin{matrix} 12 & 16 & 15 & 11 \end{matrix} \\ \begin{bmatrix} 0.166 & 0.0691 & -0.038 & -0.27 \\ 0.0691 & 0.166 & 0.13 & 0.003 \\ -0.038 & 0.13 & -0.000535 & 0.069 \\ -0.27 & .003 & 0.069 & -0.00535 \end{bmatrix} \end{array}$$

The global stiffness matrix generated is provided below:

$$k = \begin{array}{c} \begin{matrix} 1 & 2 & 3 & 4 & 5 & 6 & 7 & 8 \end{matrix} \\ \begin{bmatrix} 0.330 & -0.33 & 0.000 & 0.000 & 0.166 & -0.166 & 0.000 & 0.000 \\ +0.330 & -0.11 & 0.110 & 0.000 & 0.166 & -0.16 & 0.000 & 0.000 \\ 0.000 & 0.000 & -.053 & -0.16 & 0.00 & 0.00 & 0.055 & -.055 \\ 0.166 & -0.16 & 0.166 & -0.16 & 0.00 & 0.00 & 0.055 & -.055 \\ 0.166 & -0.16 & 0.00 & 0.000 & -0.11 & -.055 & 0.000 & 0.000 \\ 0.000 & 0.000 & 0.00 & 0.000 & -0.055 & -.885 & 0.440 & 0.000 \\ 0.000 & 0.000 & 0.055 & -.055 & 0.000 & 0.440 & -0.44 & -0.221 \\ 0.000 & 0.000 & 0.055 & -.055 & 0.000 & 0.000 & -0.22 & -.332 \\ 0.000 & 0.000 & 0.000 & 0.000 & -0.22 & -0.11 & 0.000 & 0.000 \\ 0.000 & 0.000 & 0.000 & 0.000 & 0.11 & -0.36 & 0.140 & 0.000 \\ 0.000 & 0.000 & 0.000 & 0.000 & 0.000 & 0.140 & -.223 & 0.027 \\ 0.000 & 0.000 & 0.000 & 0.000 & 0.000 & 0.000 & 0.027 & 0.083 \\ 0.000 & 0.000 & 0.000 & 0.000 & 0.000 & 0.000 & 0.000 & 0.000 \\ 0.000 & 0.000 & 0.000 & 0.000 & 0.000 & 0.000 & 0.000 & 0.000 \\ 0.000 & 0.000 & 0.000 & 0.000 & 0.000 & 0.000 & 0.000 & 0.000 \\ 0.000 & 0.000 & 0.000 & 0.000 & 0.000 & 0.000 & 0.000 & 0.000 \end{bmatrix} \end{array}$$

$$k = \begin{matrix} 9 & 10 & 11 & 12 & 13 & 14 & 15 & 16 \end{matrix}$$
$$\begin{bmatrix} 0.000 & 0.000 & 0.000 & 0.000 & 0000 & 0.000 & 0.000 & 0.000 \\ 0.000 & 0.000 & 0.000 & 0.000 & 0.000 & 0.000 & 0.000 & 0.000 \\ 0.000 & 0.000 & 0.000 & 0.000 & 0.000 & 0.000 & 0.000 & 0.000 \\ 0.000 & 0.000 & 0.000 & 0.000 & 0.000 & 0.000 & 0.000 & 0.000 \\ -0.22 & -0.11 & 0.000 & 0.000 & 0.000 & 0.000 & 0.000 & 0.000 \\ -0.11 & -0.36 & 0.14 & 0.000 & 0.000 & 0.000 & 0.000 & 0.000 \\ 0.000 & 0.140 & -0.223 & -.027 & 0.000 & 0.000 & 0.000 & 0.000 \\ 0.000 & 0.000 & -0.027 & -.083 & 0.000 & 0.000 & 0.000 & 0.000 \\ -0.44 & -0.22 & 0.000 & 0.000 & 0.000 & 0.000 & 0.000 & 0.000 \\ -0.22 & -0.995 & 0.225 & 0.000 & 0.000 & 0.000 & 0.000 & 0.000 \\ 0.000 & 0.225 & -.27 & 0.089 & 0.000 & 0.000 & 0.013 & 0.0031 \\ 0.000 & 0.000 & 0.089 & 0.032 & 0.000 & 0.000 & -0.038 & 0.0691 \\ 0.000 & 0.000 & 0.000 & 0.000 & 0.000 & 0.000 & 0.000 & 0.000 \\ 0.000 & 0.000 & 0.000 & 0.000 & 0.000 & 0.220 & 0.110 & 0.000 \\ 0.000 & 0.000 & 0.013 & -0.038 & 0.000 & 0.110 & 0.21 & -0.034 \\ 0.000 & 0.000 & 0.003 & 0.0691 & 0.000 & 0.000 & -0.34 & 0.166 \end{bmatrix}$$

For all the nine element, the value of b_i^1, b_i^2, b_i^3 was obtained using the following equation:

$$b_i^1 = 0, \tag{3.32}$$

$$b_i^2 = -\frac{1}{\left(1-\varphi+\varphi\frac{\rho_s}{\rho_f}\right)}\frac{1}{(1-\varphi)^{2.5}}\oint \psi_i q_{n2} ds, \tag{3.33}$$

$$b_i^3 = -\frac{1}{P_r}\frac{1}{\left(1-\varphi+\varphi\frac{(\rho c_p)_s}{(\rho c_p)_f}\right)}\left(\frac{k_{nf}}{k_f}\right)\oint \psi_i q_{n3} ds, \tag{3.34}$$

For element 1

$$b_1 = \begin{bmatrix} 0.0546_2 \\ 0.1102_6 \\ -0.973_5 \\ -0.486_1 \end{bmatrix},$$

For element 2

$$b_2 = \begin{bmatrix} 0_6 \\ 0.1654_{10} \\ -1.460_9 \\ -0.4866_5 \end{bmatrix} ,$$

For element 3

$$b_3 = \begin{bmatrix} -0.0546_{10} \\ 0.2206_{14} \\ -1.946_{13} \\ 0.4876_9 \end{bmatrix} ,$$

For element 4

$$b_4 = \begin{bmatrix} -0.0531_3 \\ -0.1061_7 \\ -0.759_6 \\ -0.379_2 \end{bmatrix} ,$$

For element 5

$$b_5 = \begin{bmatrix} 0_7 \\ -0.16074_{11} \\ -1.1389_{10} \\ 0_6 \end{bmatrix} ,$$

For element 6

$$b_6 = \begin{bmatrix} 0.0531_{11} \\ -0.214_{15} \\ -1.518_{14} \\ 0.379_{10} \end{bmatrix} ,$$

For element 7

$$b_7 = \begin{bmatrix} -0.1617_4 \\ -0.324_8 \\ -0.5417_7 \\ -0.271_3 \end{bmatrix} ,$$

For element 8

$$b_8 = \begin{bmatrix} 0_8 \\ -0.4867_{12} \\ -0.812_{11} \\ 0_7 \end{bmatrix} \quad ,$$

For element 9

$$b_9 = \begin{bmatrix} 0.1622_{12} \\ -0.64899_{16} \\ -1.0838_{15} \\ 0.2712_{11} \end{bmatrix}$$

Global b matrix for sixteen nodes

$$b = \begin{bmatrix} -0.4867_1 \\ -0.3244_2 \\ -0.3241_3 \\ -0.1617_4 \\ -1.460_5 \\ -0.64871_6 \\ -0.6478_7 \\ -0.324_8 \\ -0.9726_9 \\ -0.6484_{10} \\ -0.6484_{11} \\ -0.3245_{12} \\ -1.9462_{13} \\ -1.298_{14} \\ -1.297_{15} \\ -0.6489_{16} \end{bmatrix}$$

Assembly of the element equations, is used to obtain a global matrix. Further imposing boundary conditions, the system of equations is solved by the Gauss elimination method. Gaussian quadrature is implemented for solving the integration. Herein the domain $[0, \eta_{max}] \times [0, \boldsymbol{\xi}_{max}]$ is mapped into the computational domain [-1, 1] × [-1, 1].The code of the algorithm is executed in MATLAB running on a PC. The following figures show the variation of temperature along the vertical plate in 3D & 2D as well as the comparison of different thermal conductivity models.

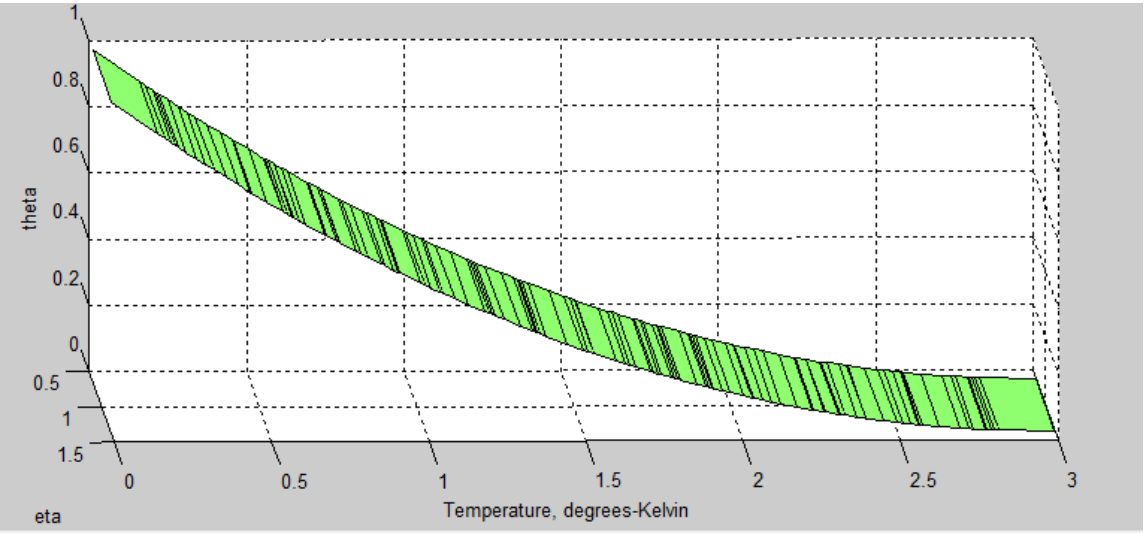

Figure 3.4: 3-D graph between theta and eta

Figure 3.4 shows the 3 D view of dimensionless temperature variation in the thermal boundary layer formed on the flat plate.

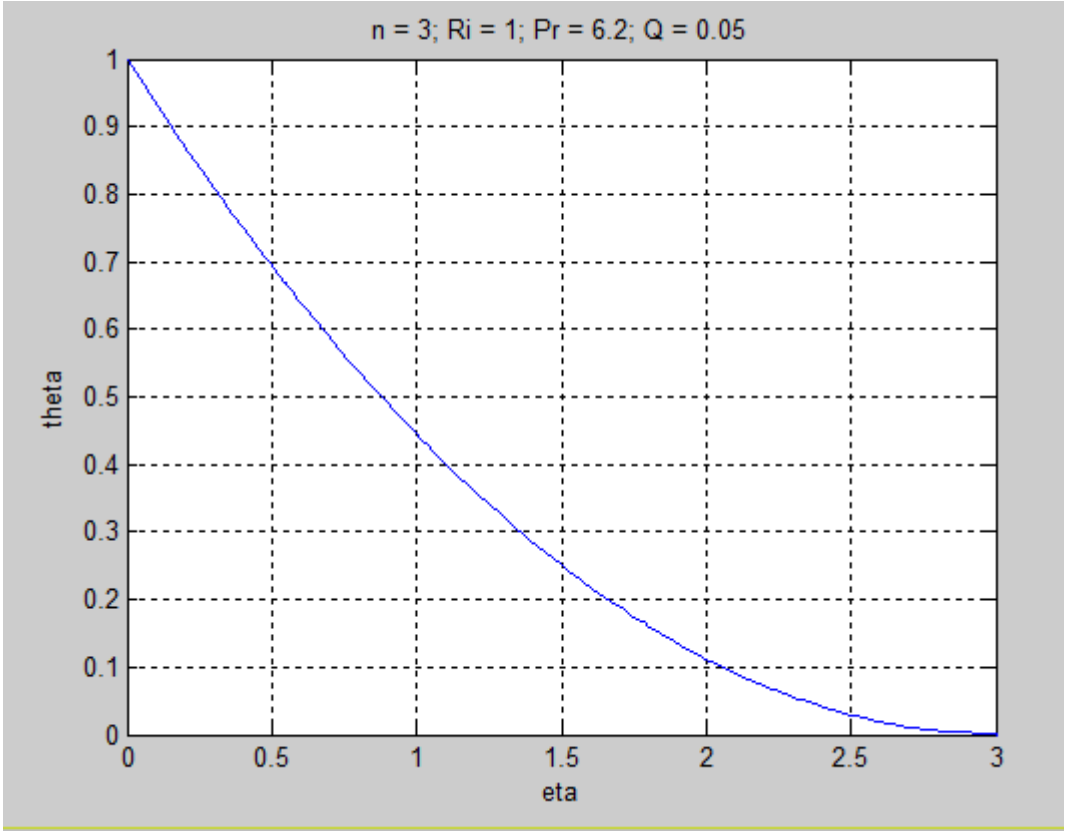

Figure 3.5: Two-dimensional graph between theta and eta

Figure 3.5 shows the 2 D view of dimensionless temperature with the variation in the thermal boundary layer formed on the flat plate.

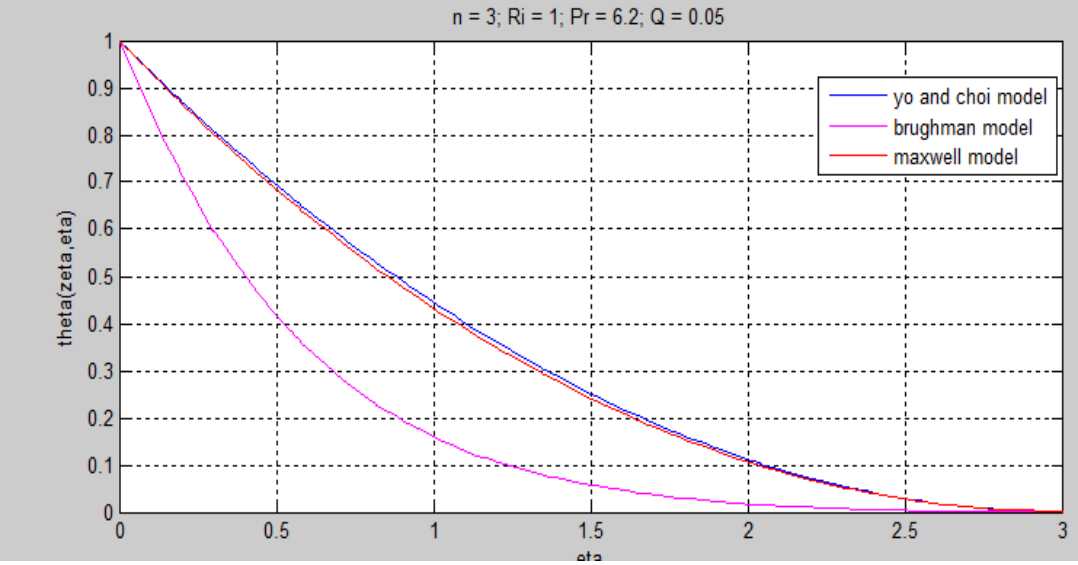

Figure 3.6: Comparison between models of thermal conductivity

In this numerical analysis, by changing the thermal conductivity models, it is found that for all the three models, the pattern of the graph is same. Maxwell model, Yo and Choi model and Bruggeman model were used for the numerical analysis. The thermal boundary layer and relative thickness of the momentum is substantially affected by Prandtl number. For Pr << 1, the momentum diffusivity is lesser than the heat diffusivity. Ri shows a significant effect in natural convection in comparison to forced convection.

Chapter 4

Experiment, Material & Method

4.1 Test Facility at Thapar University and Experimental procedure

This test facility is available in Thapar University. The KD2 Pro device is used to measure thermal conductivity of nanofluids. The thermal conductivity and resistivity is measured by single needle sensor.

4.2 Nanomaterial

The nanomaterial used in this study was Al_2O_3 –H_2O with average particle size of 30 nm and volume fraction of 1%.

4.3 Preparation of nanofluid: Sonicater

Figure 4.1: Oscar ultrasonicator

In the system surface to volume ratio is affectedly increased by small particle size. In the system energy is supplied to enhance the surface area of a material. With the help of a device known

as sonicator, the energy is generated. Sonication is used for speed dissolution by breaking intermolecular interaction. When it is impossible to stir a sample then sonicator is used. In nanotechnology for mixing the nanoparticles into the based fluid sonicator is generally used.

4.4 Thermal Property Analyzer

The KD2 Pro device is used for measuring the thermal properties of nanofluid. KD2 Pro comprises of a hand held controller and sensors which measure thermal conductivity. The single needle sensor is used to measure thermal conductivity of nanofluid. For measuring volumetric specific heat capacity, the dual needle sensor is used.

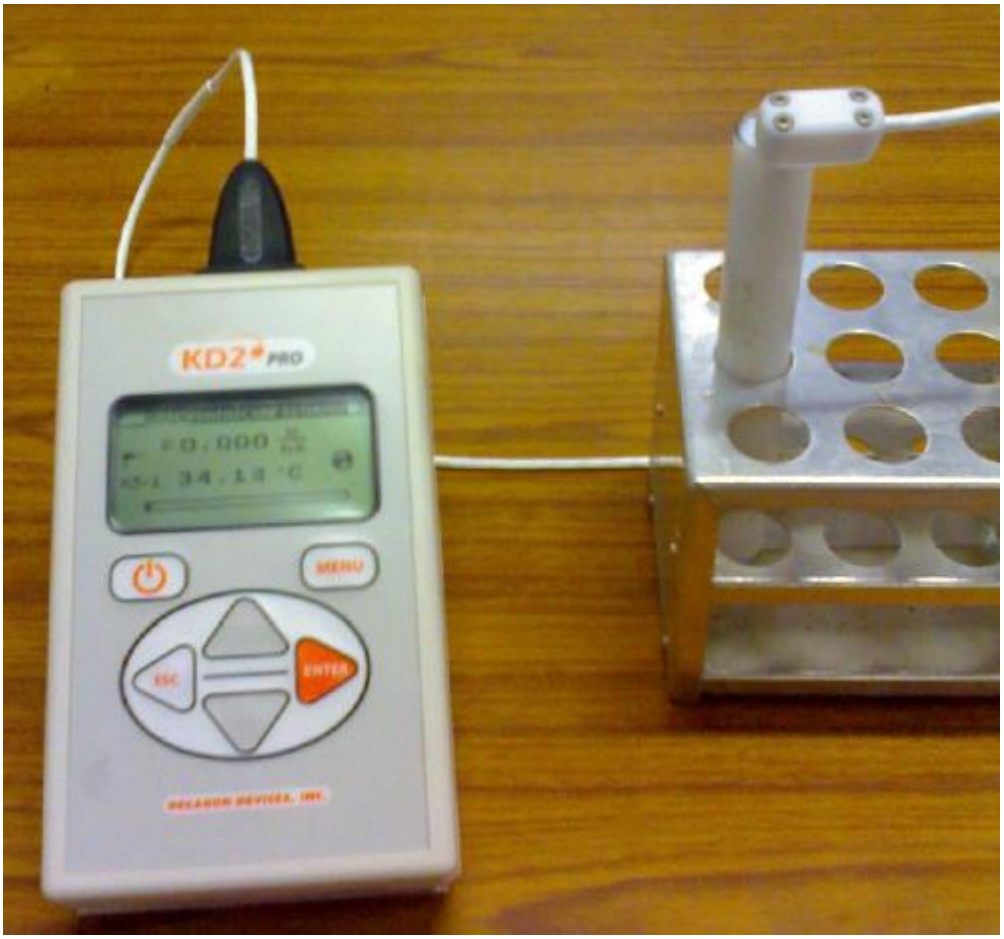

Figure 4.2: KD2 Pro

Sensors:

KS-1 single needle

KS-1 is a single needle sensor that is used to measure the thermal conductivity and resistivity of nanofluids. The size of KS-1 sensor is 60 mm long and the needle diameter is 1.3 mm. This sensor is constructed mainly for liquid sample. A very less amount of heat is supplied to the needle by the device to avoid the free convection in liquid samples. This device is not feasible for granular samples because of small size of sensor and less heating time.

Figure 4.3: KS-1 sensor needle

TR-1 single needle

TR-1 is a single needle sensor that is used to measure the thermal conductivity and resistivity of nanofluids. The size of TR-1 sensor is 100 mm long and the needle diameter is 2.4 mm. This sensor is constructed mainly for granular materials. This sensor minimizes contact resistance error due to its longer heating time and large diameter. The KS-1 sensor heats the sample lesser than TR-1. TR-1 sensor has larger diameter than KS-1 sensor due to which it is not damaged easily.

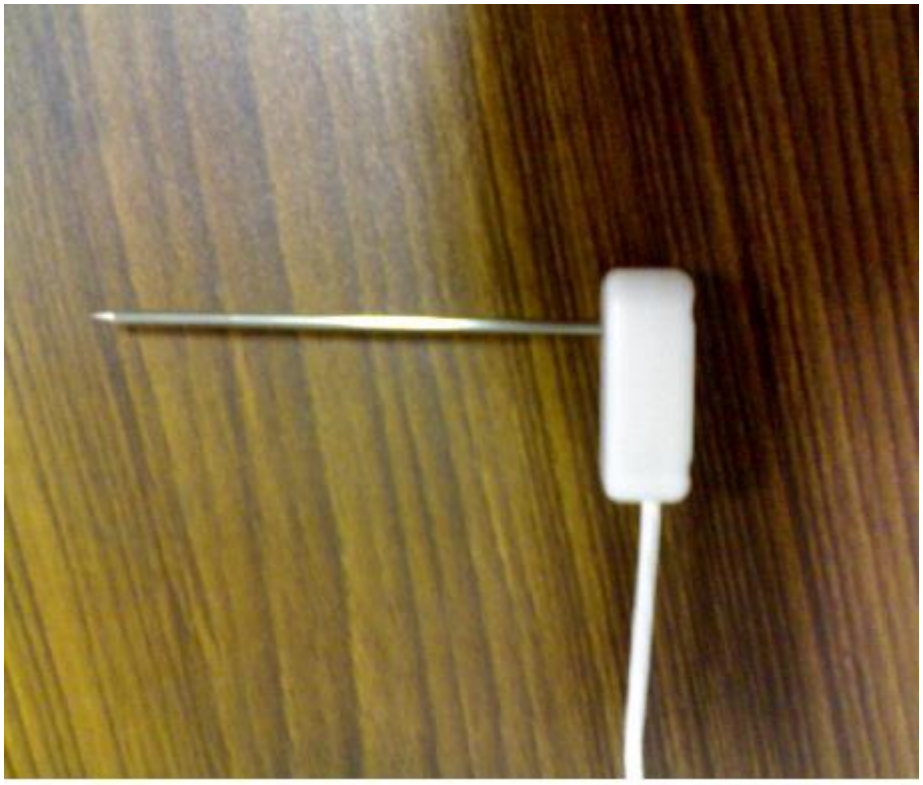

Figure 4.4: TR-1 sensor needle

SH-1dual needle

For measuring the volumetric heat capacity, thermal diffusivity, thermal conductivity and thermal resistivity, a dual needle SH-1 sensor is used. The dual needle SH-1 sensor is well suited for granular materials. This sensor is not well suited in case liquid because of large heat pulse and free convection.

.

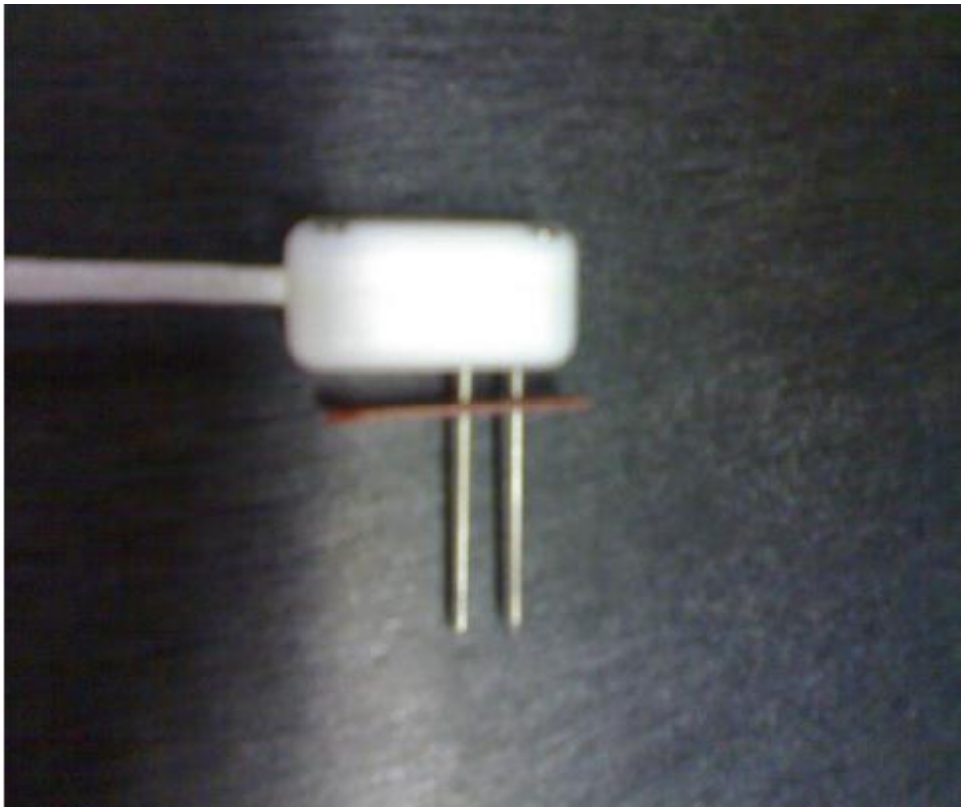

Figure 4.5: SH-1 sensor needle

4.5 Methodology

The following methodology has been used for performing the experimental work:

- The Al_2O_3 nanoparticles of average size 20-30 nm purchased.
- The nanofluids were prepared with the help of two step method i.e., by diffusing the nanoparticles in the base fluid used. In the present work, water was used as a base fluid.
- In this experiment the nanoparticles were dispersed in the base fluids in the varying volumetric concentrations by converting the volume concentrations into the mass of nanoparticles by using the law of mixtures formula.
- The correct mass of the nanoparticles as calculated by law of mixtures formula was dispersed in the base fluid by using the Sonicator for 3.5 hours.
- Then, the different types of nanofluids were prepared with varying volumetric concentrations of 0.005 %, 0.01 %, 0.05 %, 0.1 %.
- Finally, the prepared nanofluids were tested in the KD2 Pro for different volumetric concentrations, and temperatures.

- The experimental readings were taken in the tabular format. Then, for analysis the tabular data was converted into the graphical format.

Chapter 5

Results and Discussions

5.1 Experimental Results

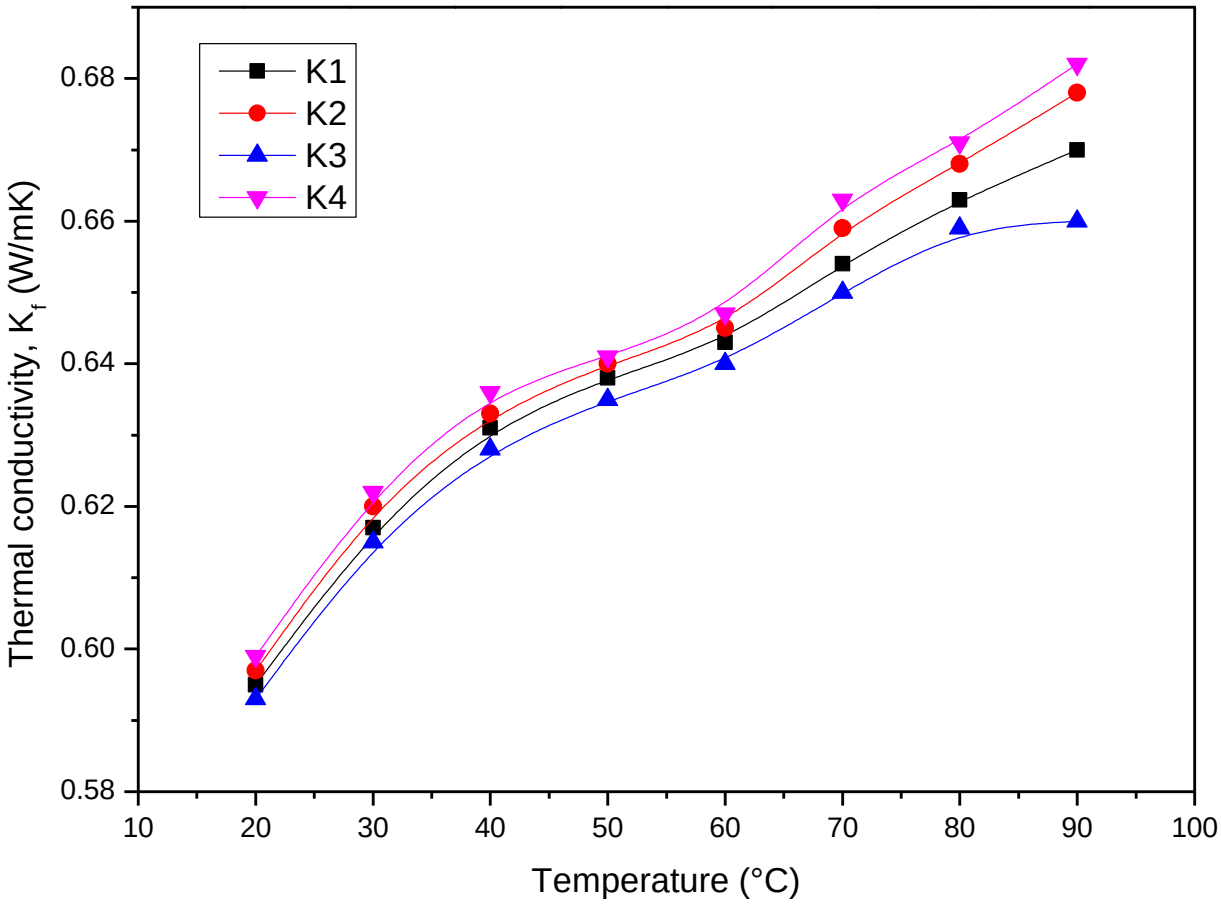

Figure 5.1: Variation of Thermal Conductivity of water with temperature

Figure 5.1 shows the variation in the thermal conductivity of fluid with temperature range 20 °C to 90 °C. At a particular temperature, the experiment was done four times. It can be observed that the thermal conductivity of fluid as well as fluid temperature increases in all the four cases. From the above figure it is justified that up to 60 °C, the error in thermal conductivity is less and between the temperature ranges 60 °C - 90 °C, high inaccuracy is observed.

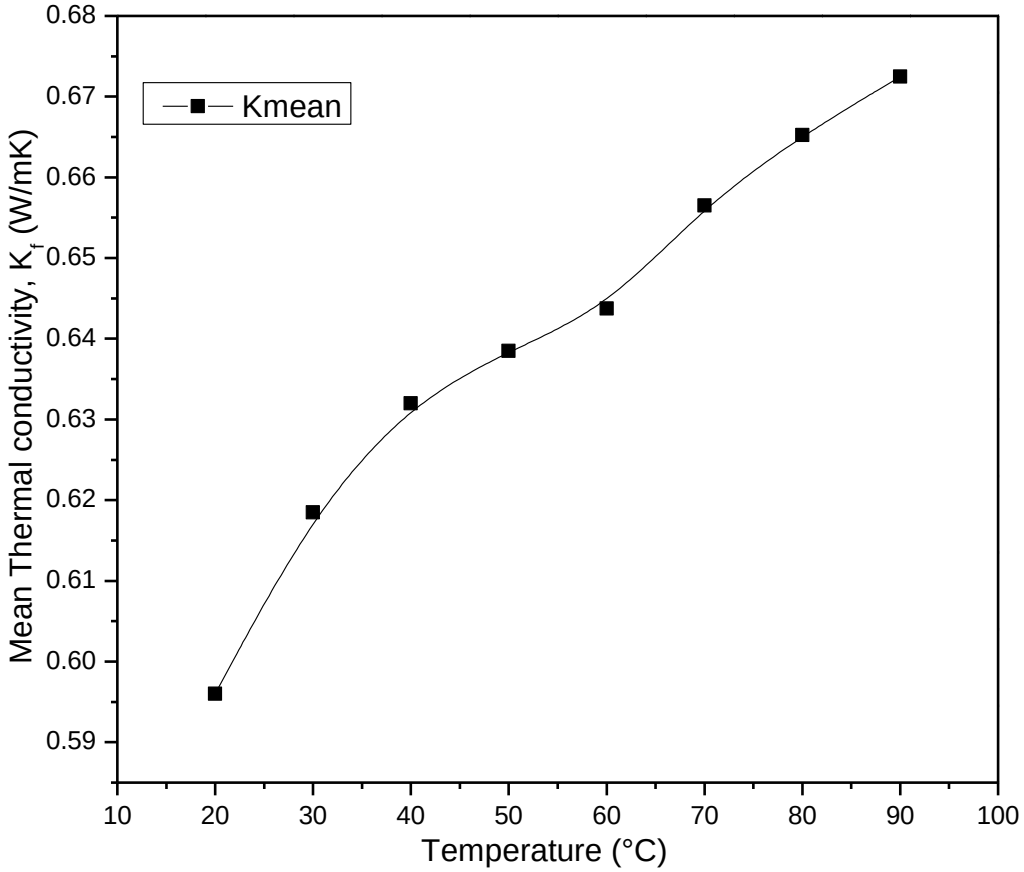

Figure 5.2: Variation of Mean Thermal Conductivity of water with temperature

Figure 5.2 shows the variation in mean thermal conductivity obtained from experiments. K_{mean} was calculated by four repeated experiments. It can be seen from the Figure 5.2 that the accuracy was good up to the temperature range 20 °C to 60 °C, however, high error is found between the ranges 60 °C to 90 °C. For the further experiments, the temperature range 20 °C to 60 °C is used.

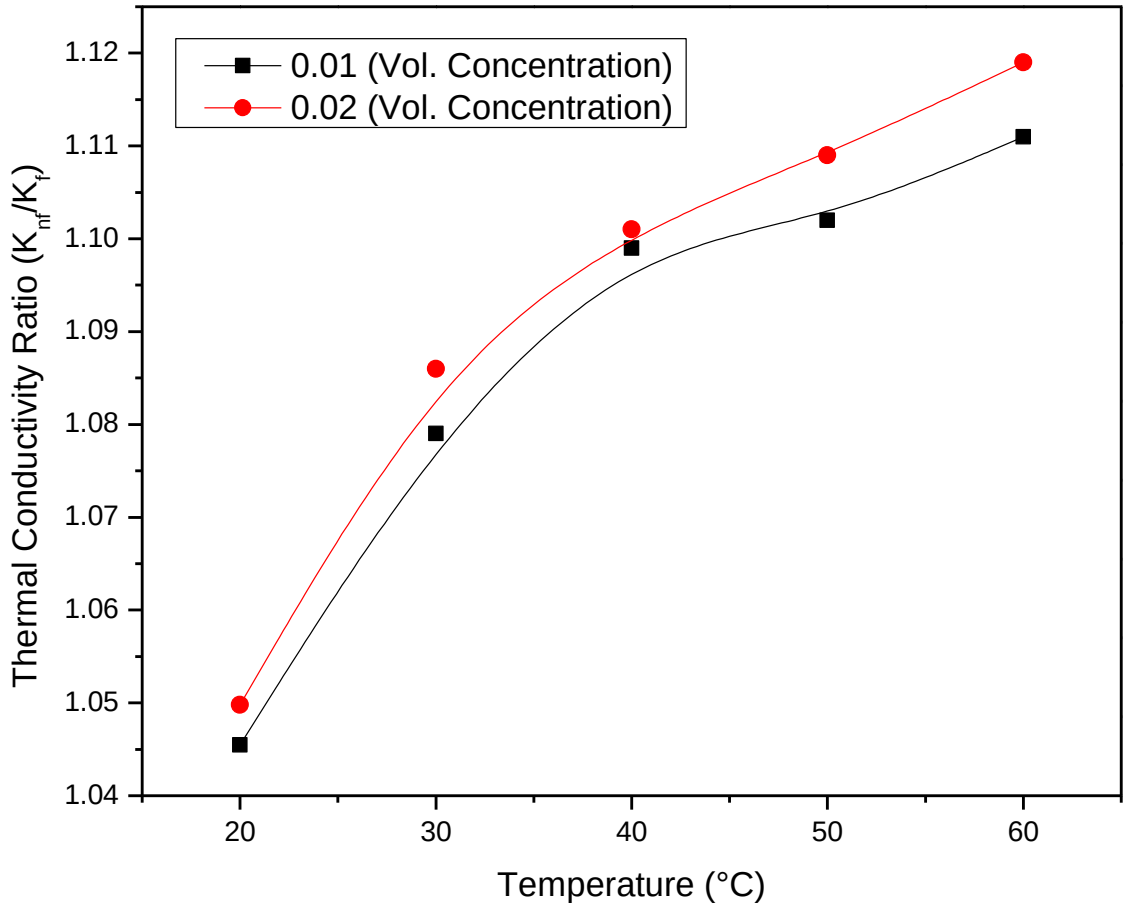

Figure 5.3: Thermal Conductivity of Al_2O_3-H_2O at 1% & 2% volumetric concentration

0Figure 5.3 shows the variation in the thermal conductivity ratio (K_{nf} /K_f) for Al_2O_3 -H_2O nanofluid at different temperature range from 20 °C to 60 °C and for the volume concentration (0.01 & 0.02). It can be observed from the given figure that the thermal conductivity ratio increases with the increase in temperature as well as with the increase in volume concentration.

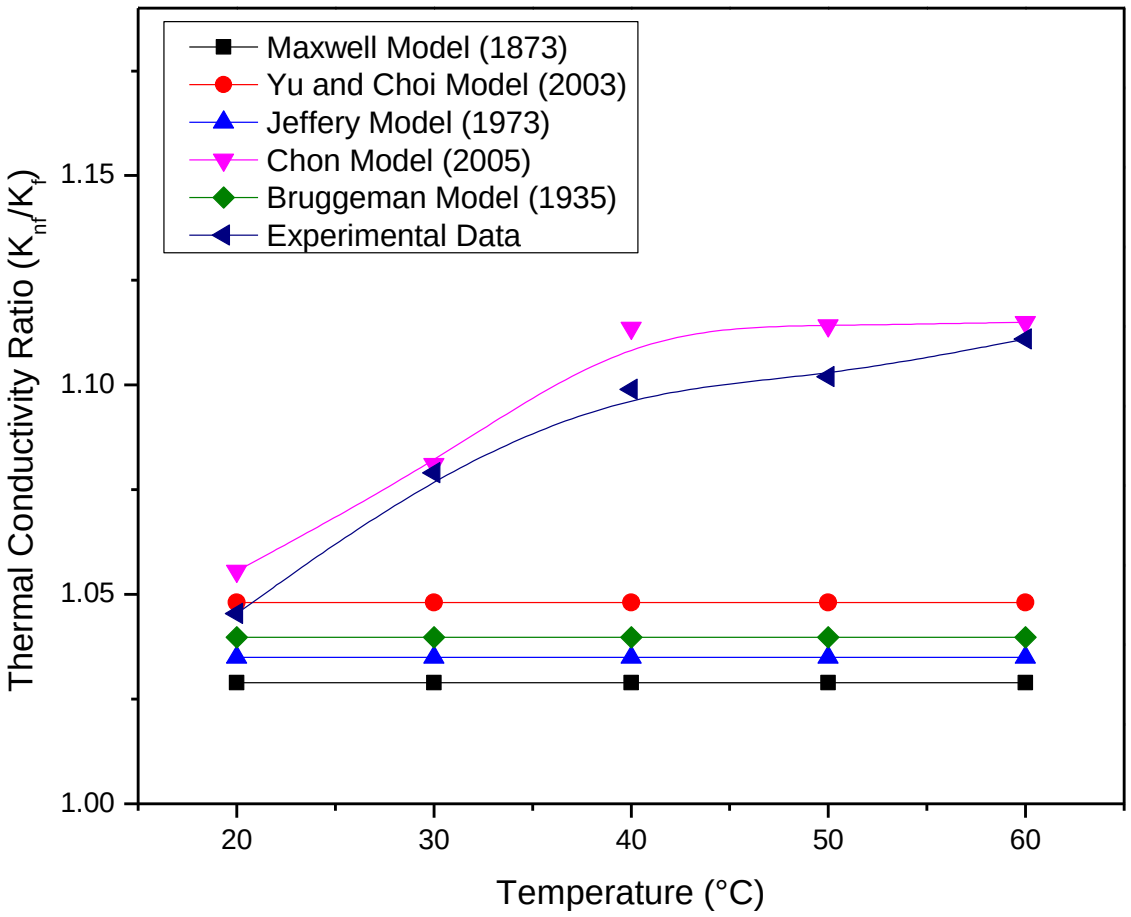

Figure 5.4: Comparison of Experimental data at (0.01) vol.concentration with empirical Models

Figure 5.4 shows the comparison between the empirical models and the experimental data results at different temperatures and at constant volume fraction (0.01).There are some models which are independent of temperature. Such models give same results at different temperature. The experimental results show good accuracy with the existing empirical models.

-

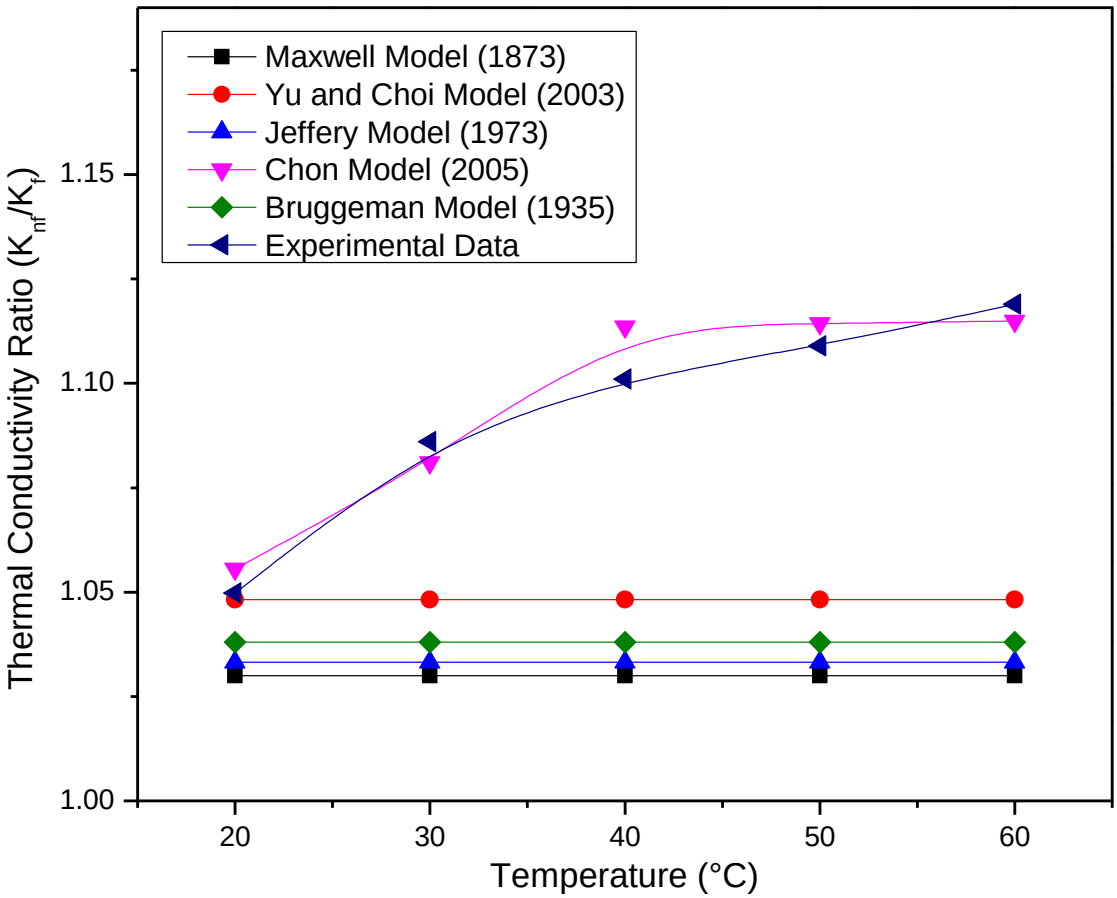

Figure 5.5: Comparison of Experimental data at (0.02) vol.concentration with empirical models

Figure 5.5 compares between the different empirical models and the experimental data results at different temperatures and constant volume fraction (0.02).There are some models which are independent of temperature. Such models give same results at different temperatures. It can be observed that the experimental results show good accuracy with the existing empirical model.

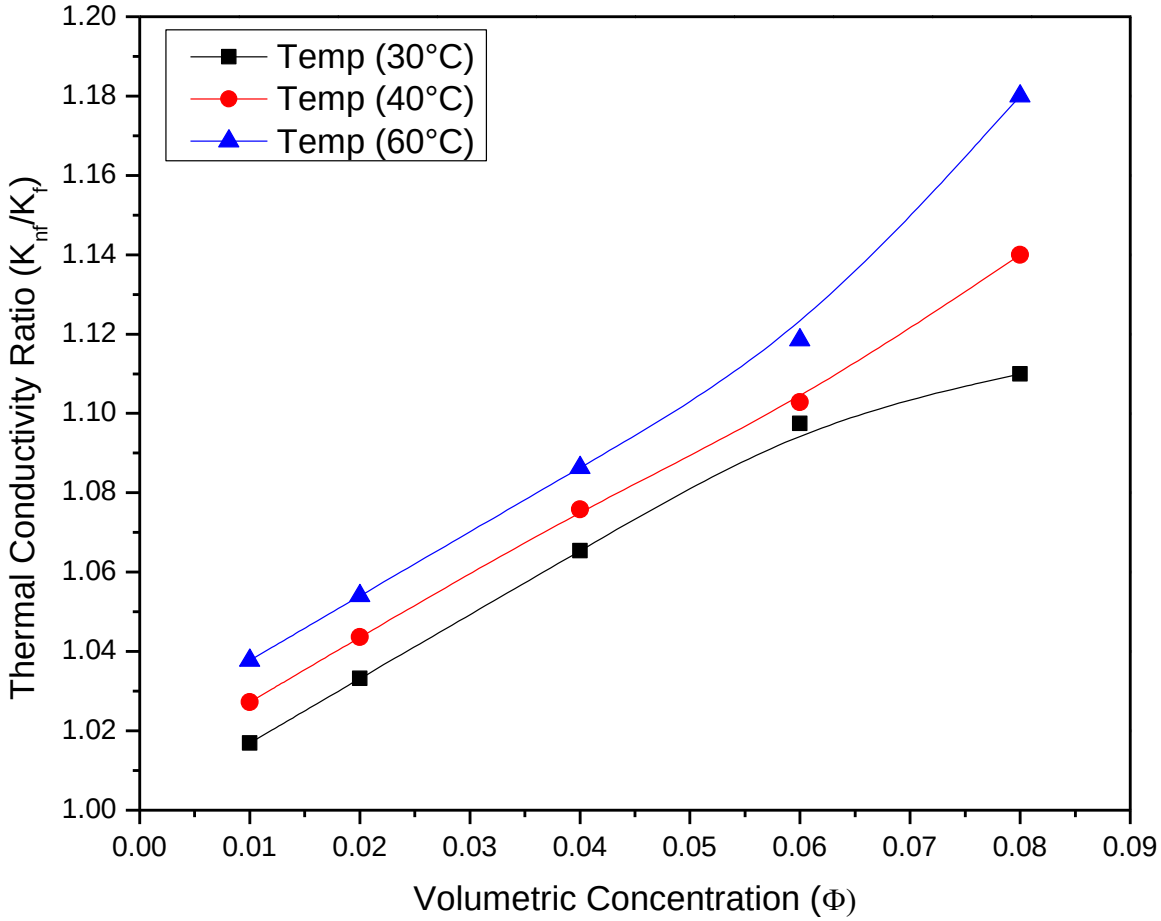

Figure 5.6: Thermal Conductivity of Al_2O_3-H_2O at different volumetric concentration

Figure 5.6 shows the variation in the thermal conductivity ratio (K_{nf} /K_f) for the Al_2O_3-H_2O nano fluid for different volume concentrations ranging from 0.02 to 0.08 and for the temperature ranges 30°C to 60°C. It can be observed that the thermal conductivity ratio increases with the increase in volumetric concentration and temperature.

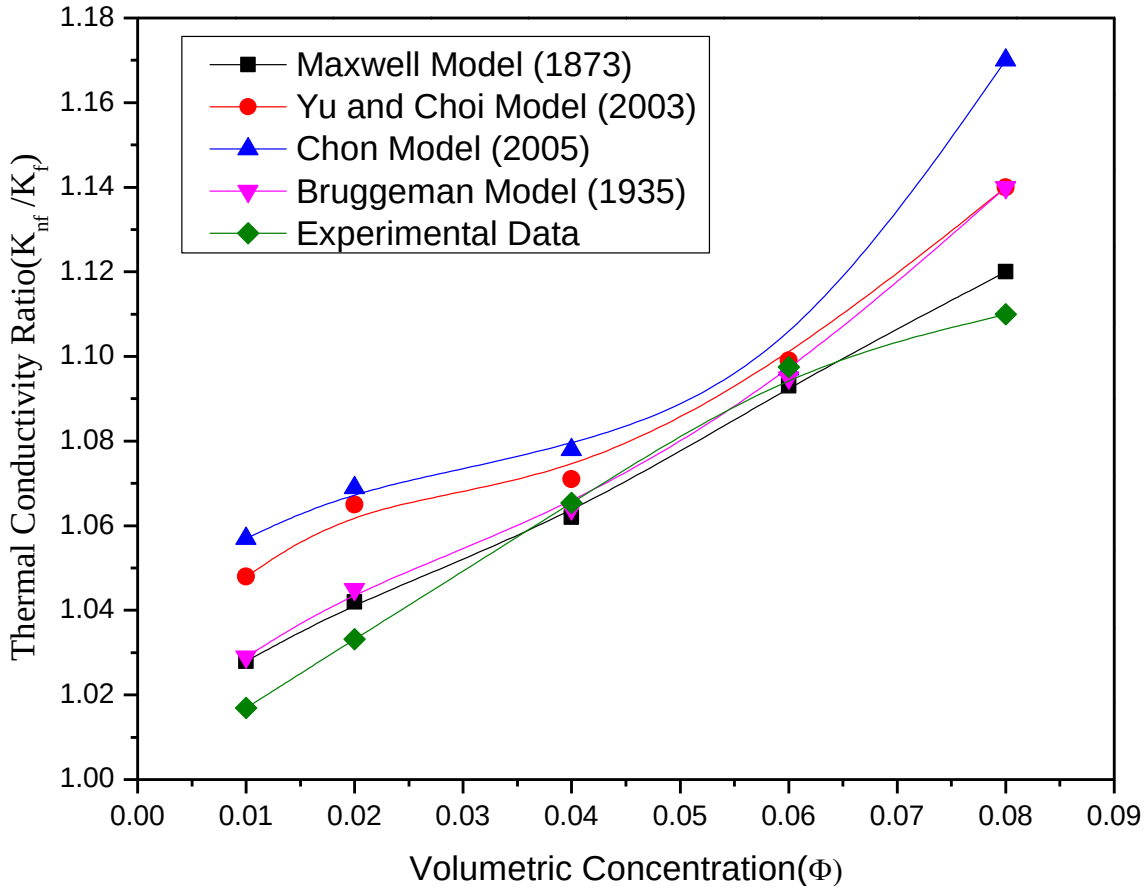

Figure 5.7: Comparison of Experimental data at (30°C) with empirical Models for different vol. concentration

Figure 5.7 shows the comparison between different empirical models and the experimental results with different values of thermal conductivity ratio for varying volume fractions at 40 °C. It can be observed from the Figure 5.8 that the experimental results show good accuracy with the existing empirical model.

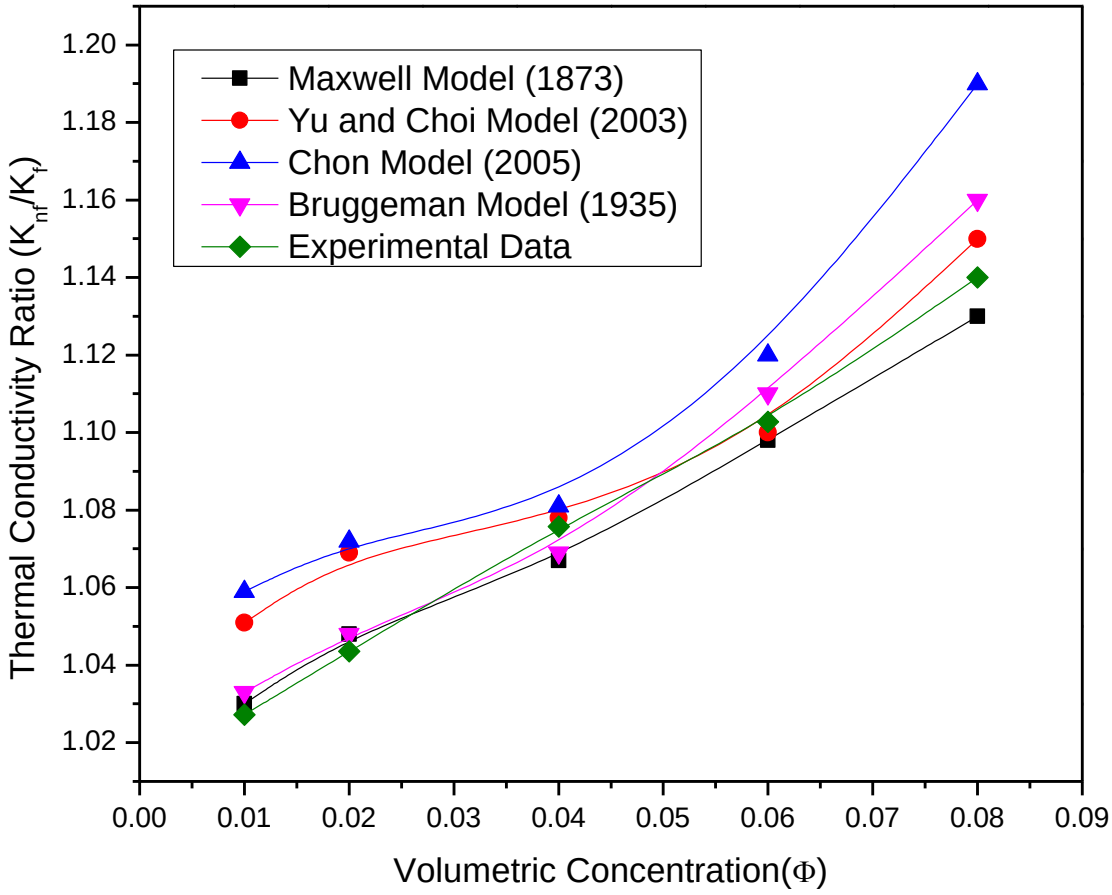

Figure 5.8: Comparison of Experimental data at (40°C) with empirical Models for different vol. concentration

Figure 5.8 shows the comparison between different empirical models and the experimental results with different values of thermal conductivity ratio for varying volume fractions at 40 °C. It can be observed from the Figure 5.8 that the experimental results show good accuracy with the existing empirical model.

Chapter 6

Conclusion & Future Scope

6.1 Conclusion

The work done in the present thesis was expected to get Finite element solution of some nonlinear problems arising because of transport phenomena in nanofluids in various geometries.

- Partial differential equations have been obtained successfully for the performance of nanofluid over a flat plate.
- The governing equations have been solved by using MATLAB and FEM.
- Nature of the temperature plots obtained from the numerical investigation into the performance of nanofluid are found to be tracking well the expected physics.
- The experimental study on thermal conductivity of nanofluid shows that thermal conductivity ratio (K_{nf}/K_f) increases with increase in temperature and volumetric concentration.
- KD2 Pro analyzer is optimal for the temperature range (20°C to 60°C). For high temperature ranges, it shows maximum error.

6.2 Future Scope

There is sufficient scope to extend this work in multi-directions. Some of conceivable choices are listed below.

- An investigation of turbulent nanofluid flow issues with consideration of other slip mechanism viz. inertia, drag force and Magnus force, may be undertaken.
- Due to different biomedical use of nanofluids e.g. controlling the drug delivery, as tumor therapeutics, the numerical simulation of these type of bio-medical issues should be possible by catching bio-fluid as base fluid.
- This work can be continued to other base fluid e.g. engine oil and polymer with both magnetic and non-magnetic nanoparticles.

- Since KD2 Pro gives inaccurate results at high temperature, therefore some other thermal conductivity measuring equipment could be employed with experiments for better results.

References

Bourantas, G.C., Skouras, E.D., Loukopoulos, V.C. and Burganos, V.N., 2014. Heat transfer and natural convection of nanofluids in porous media. *European Journal of Mechanics-B/Fluids*, *43*, pp.45-56.

Buongiorno, J., 2006. Convective transport in nanofluids. Journal of Heat Transfer, 128(3), pp.240-250.

Chen, H., Ding, Y. and Lapkin, A., 2009. Rheological behaviour of nanofluids containing tube/rod-like nanoparticles. Powder Technology, 194(1), pp.132-141.

Chen, H., Ding, Y., He, Y. and Tan, C., 2007. Rheological behaviour of ethylene glycol based titania nanofluids. Chemical Physics Letters, 444(4), pp.333-337.

Choi, S.P.J.S., 2007. Effects of various parameters on nanofluids. Thermal conductivity. Journal of Heat Transfer, 129, p.6.

Chol, S.U.S., 1995. Enhancing thermal conductivity of fluids with nanoparticles. ASME-Publications-Fed, 231, pp.99-106.

Chon, C.H., Kihm, K.D., Lee, S.P. and Choi, S.U., 2005. Empirical correlation finding the role of temperature and particle size for nanofluid (Al 2 O 3) thermal conductivity enhancement. Applied Physics Letters, 87(15), p.153107.

Dandapat, B.S. and Gupta, A.S., 1989. Flow and heat transfer in a viscoelastic fluid over a stretching sheet. International Journal of Non-Linear Mechanics, 24(3), pp.215-219.

Das S.K., Choi S.U.S., Yu W. and Pradeep K., 2007, Nanofluids Science and Technology, Publ. Wiley Interscience.

Das S.K., Putra N., Thiesen P. and Roetzel W., 2003, Temperature Dependence of Thermal Conductivity Enhancement for Nanofluids, Heat Transfer, Vol. 125, PP. 567-574.

Das, S.K., Choi, S.U., Yu, W. and Pradeep, T., 2007. Nanofluids: science and technology. John Wiley & Sons.

Eastman, J.A., Choi, U.S., Li, S., Thompson, L.J. and Lee, S., 1996. Enhanced thermal conductivity through the development of nanofluids. In MRS proceedings (Vol. 457, p. 3). Cambridge University Press.

Ferdows, M., Khan, M.S., Alam, M.M. and Sun, S., 2012. MHD mixed convective boundary layer flow of a nanofluid through a porous medium due to an exponentially stretching sheet. Mathematical problems in Engineering, 2012.

Gorla, R.S.R., Chamkha, A.J. and Rashad, A.M., 2011. Mixed convective boundary layer flow over a vertical wedge embedded in a porous medium saturated with a nanofluid: natural convection dominated regime. Nanoscale research letters, 6(1), p.207.

Jang, S.P. and Choi, S.U., 2006. Cooling performance of a microchannel heat sink with nanofluids. Applied Thermal Engineering, 26(17), pp.2457-2463.

Kamyar, A., Saidur, R. and Hasanuzzaman, M., 2012. Application of computational fluid dynamics (CFD) for nanofluids. *International Journal of Heat and Mass Transfer*, *55*(15), pp.4104-4115.

Karthikeyan, N.R., Philip, J. and Raj, B., 2008. Effect of clustering on the thermal conductivity of nanofluids. Materials Chemistry and Physics, 109(1), pp.50-55.

Keblinski, P., Eastman, J.A. and Cahill, D.G., 2005. Nanofluids for thermal transport. Materials today, 8(6), pp.36-44.

Khan, W.A. and Gorla, R.S.R., 2011. Heat and mass transfer in non-Newtonian nanofluids over a non-isothermal stretching wall. Proceedings of the Institution of Mechanical Engineers, Part N: Journal of Nanoengineering and Nanosystems, 225(4), pp.155-163.

Koo, J. and Kleinstreuer, C., 2004. A new thermal conductivity model for nanofluids. Journal of Nanoparticle Research, 6(6), pp.577-588.

Koo, J. and Kleinstreuer, C., 2005. Laminar nanofluid flow in microheat-sinks. International Journal of Heat and Mass Transfer, 48(13), pp.2652-2661.

Koo, J., 2005. Computational nanofluid flow and heat transfer analyses applied to micro-systems.

Leong, K.C., Yang, C. and Murshed, S.M.S., 2006. A model for the thermal conductivity of nanofluids–the effect of interfacial layer. Journal of nanoparticle research, 8(2), pp.245-254.

Li C. H. and Peterson G. P., 2007,The effect of particle size on the effective thermal conductivity of Al_2O_3-water nanofluids, Applied physics, Vol. 101, Issue. 044312, PP. 1-5.

Li, J., 2008. Computational analysis of nanofluid flow in microchannels with applications to micro-heat sinks and bio-MEMS.

Li, S. and Eastman, J.A., 1999. Measuring thermal conductivity of fluids containing oxide nanoparticles. J. Heat Transf, 121(2), pp.280-289.

Masuda, H., Ebata, A. and Teramae, K., 1993. Alteration of thermal conductivity and viscosity of liquid by dispersing ultra-fine particles. Dispersion of Al2O3, SiO2 and TiO2 ultra-fine particles.

Maxwell, J.C., 1881. A treatise on electricity and magnetism (Vol. 1). Clarendon press.[110]

Mintsa H.A., Roy G. and Nguyen C.T., 2007, New Temperature Dependent Thermal Conductivity Data of Water Based Nanofluids, 5th IASME/WSEAS Int. Conference on Heat Transfer, Thermal Engineering and Environment, Athens, Greece, PP. 290-294.

Murshed S.M.S., Leong K.C. and Yang C., 2005,Enhanced thermal conductivity of TiO2—water based nanofluids, International Journal of Thermal Sciences, Vol. 44, PP. 367–373.

Murshed, S.M.S., Leong, K.C. and Yang, C., 2008. Investigations of thermal conductivity and viscosity of nanofluids. International Journal of Thermal Sciences, 47(5), pp.560-568.

Nield, D.A. and Kuznetsov, A.V., 2009. The Cheng–Minkowycz problem for natural convective boundary-layer flow in a porous medium saturated by a nanofluid. International Journal of Heat and Mass Transfer, 52(25), pp.5792-5795.

Oztop, H.F. and Abu-Nada, E., 2008. Numerical study of natural convection in partially heated rectangular enclosures filled with nanofluids. *International Journal of Heat and Fluid Flow*, *29*(5), pp.1326-1336.

Pak, B.C. and Cho, Y.I., 1998. Hydrodynamic and heat transfer study of dispersed fluids with submicron metallic oxide particles. Experimental Heat Transfer an International Journal, 11(2), pp.151-170.

Pfautsch, E., 2008. Forced convection in nanofluids over a flat plate (Doctoral dissertation, University of Missouri--Columbia).

Prakash, M. and Giannelis, E.P., 2007. Mechanism of heat transport in nanofluids. Journal of computer-aided materials design, 14(1), pp.109-117.

Prasher, R., Bhattacharya, P. and Phelan, P.E., 2006. Brownian-motion-based convective-conductive model for the effective thermal conductivity of nanofluids. Journal of heat transfer, 128(6), pp.588-595.

Rajagopal, K.R., Na, T.Y. and Gupta, A.S., 1984. Flow of a viscoelastic fluid over a stretching sheet. Rheologica Acta, 23(2), pp.213-215.

Rajagopal, K.R., Na, T.Y. and Gupta, A.S., 1987. A non-similar boundary layer on a stretching sheet in a non-Newtonian fluid with uniform free stream. J. Math. Phys. Sci, 21(2), pp.189-200.

Rao, B.N., 1996. Flow of a fluid of second grade over a stretching sheet. International journal of non-linear mechanics, 31(4), pp.547-550.

Saidur, R., Leong, K.Y. and Mohammad, H., 2011. A review on applications and challenges of nanofluids. Renewable and sustainable energy reviews, 15(3), pp.1646-1668.

Savithiri, S., Pattamatta, A. and Das, S.K., 2011. Scaling analysis for the investigation of slip mechanisms in nanofluids. Nanoscale research letters, 6(1), p.471.

Sheikholeslami, M., Gorji-Bandpy, M. and Soleimani, S., 2013. Two phase simulation of nanofluid flow and heat transfer using heatline analysis. *International Communications in Heat and Mass Transfer*, *47*, pp.73-81.

Sheu, L.J., 2011. Thermal instability in a porous medium layer saturated with a viscoelastic nanofluid. Transport in porous media, 88(3), pp.461-477.

Wang, X., Xu, X. and S. Choi, S.U., 1999. Thermal conductivity of nanoparticle-fluid mixture. Journal of thermophysics and heat transfer, 13(4), pp.474-480.

Yu, C.J., Richter, A.G., Datta, A., Durbin, M.K. and Dutta, P., 1999. Observation of molecular layering in thin liquid films using X-ray reflectivity. Physical Review Letters, 82(11), p.2326.

Yu, W. and Xie, H., 2012. A review on nanofluids: preparation, stability mechanisms, and applications. Journal of Nanomaterials, 2012, p.1.

Yu, W., France, D.M., Routbort, J.L. and Choi, S.U., 2008. Review and comparison of nanofluid thermal conductivity and heat transfer enhancements. Heat Transfer Engineering, 29(5), pp.432-460.

Zhang X., and FujiiM., 2000, Simultaneous Measurements of the ThermalConductivity and Thermal Diffusivity of MoltenSalts with a Transient Short-Hot-Wire MethodInternational Journal of Thermophysics, Vol. 21, Issue. 1, PP. 71-84.

Appendix A

For a rectangular geometry, there are four nodes and the value of shape function at each node is given below.

$\psi_1 = \frac{1}{4}(1-\xi)(1-\eta)$

$\psi_2 = \frac{1}{4}(1+\xi)(1-\eta)$

$\psi_3 = \frac{1}{4}(1+\xi)(1+\eta)$

$\psi_4 = \frac{1}{4}(1-\xi)(1+\eta)$

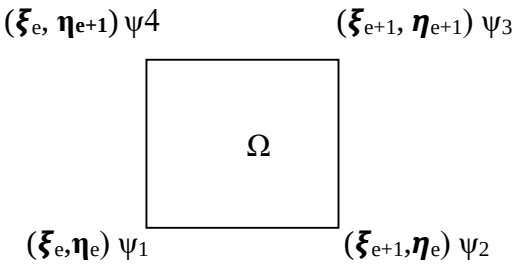

Element equation $k_{ij}^{23} = Ri \int \psi_i \xi \, \psi_j d\xi d\eta,$

Put i= 1,2,3,4 and varying the value of j (1, 2, 3, 4) for each value of i. Then, we get a 4*4 matrix for this element. Taking the value of Ri=1 for this problem.

Put i=1, j=1

$k_{11}^{23} = Ri \int \psi_1 \xi \, \psi_1 d\xi d\eta,$

$= Ri \int \frac{1}{4}(1-\xi)(1-\eta)\xi \frac{1}{4}(1-\xi)(1-\eta) d\xi d\eta,$

$= Ri \int \frac{1}{16}(1-\xi)^2 \xi \, (1-\eta)^2 d\xi d\eta$

= - 0.22

Put i=1, j=2

$k_{12}^{23} = Ri \int \psi_1 \xi \, \psi_2 d\xi d\eta$

$= Ri \int \frac{1}{4}(1-\xi)(1-\eta)\xi \frac{1}{4}(1+\xi)(1-\eta) d\xi d\eta,$

= 0

$k_{13}^{23} = Ri \int \psi_1 \xi \, \psi_3 d\xi d\eta$ =0

$k_{14}^{23} = Ri \int \psi_1 \xi \, \psi_4 d\xi d\eta$ = -0.111

$k_{21}^{23} = Ri \int \psi_2 \xi \, \psi_1 d\xi d\eta$ = 0

$k_{22}^{23} = Ri \int \psi_2 \xi \, \psi_2 d\xi d\eta$ = 0.22

$k_{23}^{23} = Ri \int \psi_2 \xi \, \psi_3 d\xi d\eta$ = 0.11

$k_{24}^{23} = Ri \int \psi_2 \xi \, \psi_4 d\xi d\eta$ =0

$k_{31}^{23} = Ri \int \psi_3 \xi \, \psi_1 d\xi d\eta$ =0

$k_{32}^{23} = Ri \int \psi_3 \xi \psi_2 d\xi d\eta$ =0.11

$k_{33}^{23} = Ri \int \psi_3 \xi \psi_3 d\xi d\eta$ =0.22

$k_{34}^{23} = Ri \int \psi_3 \xi \psi_4 d\xi d\eta$ =0

$k_{41}^{23} = Ri \int \psi_4 \xi \psi_1 d\xi d\eta$ = -0.11

$k_{42}^{23} = Ri \int \psi_4 \xi \psi_2 d\xi d\eta$ =0

$k_{43}^{23} = Ri \int \psi_4 \xi \psi_3 d\xi d\eta$ =0

$k_{44}^{23} = Ri \int \psi_4 \xi \psi_4 d\xi d\eta$ =-0.22

$$K^{23} = \begin{bmatrix} -0.22 & 0 & 0 & -0.11 \\ 0 & 0.22 & 0.11 & 0 \\ 0 & 0.11 & 0.22 & 0 \\ -0.11 & 0 & 0 & -0.22 \end{bmatrix}$$

K^{23} is a symmetric matrix.